

Chapter 6

**ACCURATE GPS-BASED GUIDANCE
OF AGRICULTURAL VEHICLES OPERATING
ON SLIPPERY GROUND**

Benoit Thuilot^{1}, Roland Lenain^{2†},*

Philippe Martinet¹ and Christophe Cariou²

¹LASMEA, Clermont-Ferrand University, 24 avenue des Landais,
63177 Aubièrre Cedex FRANCE

²CEMAGREF Institute, 24 avenue des Landais - BP 50085
63172 Aubièrre Cedex FRANCE

Abstract

The development of automatic guidance systems for agricultural vehicles is receiving a large attention from both researchers and manufacturers. The motivations in such automated devices are, on one hand, to reduce considerably the arduous driving task, and on the other hand, to improve the efficiency and the quality of the agronomic work carried out.

Such guidance devices require realtime vehicle localization on an unstructured area, such as agricultural fields. Nowadays, RTK GPS sensor appears as a very suitable sensor for these applications, since it can supply this information with a satisfactory centimeter accuracy at a high 10 Hz frequency, without requiring any preliminary equipment of the field.

In this chapter, it is demonstrated that very accurate curved path following can actually be achieved by agricultural vehicles, even on slippery ground, relying on a single RTK GPS sensor.

In a first step, in order to benefit from recent advances in Control Theory, sliding effects have been omitted, and therefore guidance laws have first been designed relying

*E-mail address: Benoit.Thuilot@lasmea.univ-bpclermont.fr

†E-mail address: Roland.Lenain@cemagref.fr

on a vehicle kinematic model. More precisely, taking advantage from structural properties of these models (they can be converted into a so-called chained form), curved path following has been achieved by designing a non-linear control law. Full-scale experiments reveal a very satisfactory guidance accuracy, except when the vehicle enters into sharp curves or when it moves on sloping fields.

In these two latter situations, guidance accuracy is damaged since the vehicle undergoes sliding effects. In agricultural applications, vehicle dynamic models appear untractable from the control design point of view. Therefore, it is here proposed to describe sliding effects as a structured perturbation acting on vehicle kinematic model. Adaptive Control framework, and more precisely Internal Model techniques, can then be used jointly with the above mentioned non-linear control law to reject sliding effects, when still preserving all the advantages of the previously designed non-linear guidance law.

Experiments demonstrate satisfactory guidance accuracy when the vehicle moves along a slope or when it executes sharp curves, excepted at their beginning or end. These transient guidance errors mainly ensue from delays introduced by the actuation device. Since the shape of the path to be followed is known, beginning/end of curves or slopes can be anticipated. Model Predictive Control framework is here used to provide such an anticipation. Satisfactory experimental results display the performances of the overall control scheme.

1 Introduction

The development of guidance systems for agricultural vehicles receives more and more attention from researchers and manufacturers. The objectives and the motivations are numerous, since automatic guidance:

- reduces the work arduousness: for instance, achieving perfectly parallel runs when driving manually, is very tiring over hours.
- allows the driver to fully devote his time to the monitoring and the tuning of the tool. This clearly can improve the quality of the agronomic work carried out.
- ensures an optimal work precision all day long and on the whole field. Double applied and skipped areas between successive passages can then be minimized, so that the exact placement of field inputs (seeds, fertilizers, pesticides, etc.) can be achieved. Their cost can then be reduced, and their environmental-unfriendly features (e.g. when pesticides are considered) can be supervised.
- allows to operate wider tools at higher speeds. Therefore productivity can be increased.

Such guidance devices require realtime vehicle localization on an unstructured area, such as agricultural fields. Nowadays, it can be supplied very satisfactorily by an *RTK-GPS sensor (RealTime Kinematic - Global Positioning System)*: absolute 3D-localization information is available at a 10 Hz frequency with a centimeter accuracy. This frequency, as well as this accuracy, are clearly suitable for vehicle guidance applications.

This sensor appears very attractive, since no preliminary field equipment is required (there is no need for buried-cables, magnets or beacons sets, etc., such as with some other localization devices), and information can be provided whatever the weather or the light conditions (localization can be obtained by night, in presence of dust, etc., which is not the case for instance with a camera sensor). Moreover, this sensor is here fully reliable, since interruptions in GPS signal reception, which is one major concern, do not occur in agricultural tasks where vehicles move on open fields.

Therefore, the RTK GPS sensor is now frequently considered to address vehicles guidance applications. It is usually the keystone of a perception device enclosing multiple sensors. For instance, in agricultural literature, guidance applications have been reported relying on a GPS and a fiber optic gyroscope (FOG) [12], a GPS, a camera and near infrared reflectance sensors [16], or multiple GPS antennas [13]. Similar approaches are also developed in Japanese universities [20].

Moreover, some companies are already marketing some guidance systems relying on an RTK GPS sensor. The first commercial device dedicated to agricultural use, has been introduced in 1997 by the Australian company *AgSystems*. This device, named *BEELINE Navigator*, consists in an RTK GPS sensor coupled with an Inertial Navigation System (INS), and is mainly dedicated to achieve perfect straight runs. In the U.S.A., this market is currently led by the company *Novariant* (previously *IntegriNautics*). Their *AutoSteer System* relies on a 3-antennas RTK GPS sensor, that can provide the whole tractor attitude. Therefore, curved path following can also be addressed. GPS systems suppliers as well as agricultural manufacturers are also investing in this market: *Trimble* is selling the *AgGPS Autopilot*, relying mainly on their *AgGPS 214* and now *AgGPS 252* RTK-GPS sensors, when manufacturer *John Deere* has established partnerships with the university of Illinois and Stanford university, and is now marketing the *AutoTrac* system, relying on their *StarFire* RTK GPS receiver. These two systems are also mainly dedicated to achieve straight line following. Additional inertia sensors allow to compensate GPS information for slope.

These research works and commercial products show clearly the interests in vehicle automatic guidance dedicated to agricultural tasks, and the relevancy of the RTK GPS sensor to address such applications.

Automatic guidance of agricultural vehicles is then addressed here, with the aim to propose enhanced capabilities, and relying nevertheless solely on an 1-antenna RTK GPS sensor.

Firstly, it has been above mentioned that most of marketed devices are currently devoted to applications where the vehicles must execute perfectly straight lines (e.g. row cropping, harvesting, ...). Extending guidance systems capabilities in order that the vehicles could also follow curved paths would be of practical interest (in order to achieve automatic half-turns, field boundaries following, etc.).

Secondly, if the vehicles are expected to achieve curved paths on agricultural fields, they will inevitably undergo sliding effects. Therefore, if high accurate guidance is the objective, it appears necessary to characterize the influence of such effects on the vehicle motion, and

to account for sliding phenomenon in guidance laws. The same conclusion has also to be derived if the vehicles are expected to perform straight lines on sloping fields.

Finally, it can also be observed that most of the above-mentioned guidance systems either described in the literature, or already marketed, rely on several sensors. Such an equipment is efficient since it provides control designers with numerous information on the vehicle attitude (or even with the whole vehicle attitude if a 3-antennas RTK GPS sensor is considered), but is quite expensive. It is therefore interesting to investigate first the guidance accuracy that could be expected when relying solely on an 1-antenna RTK GPS sensor.

The application considered here is then vehicles guidance along arbitrary curved paths, on agricultural fields where sliding is likely to occur. Our aim is to achieve high accuracy guidance relying solely on a 1-antenna RTK GPS sensor.

The approach presented here relies, on one hand on modeling developments, and on the other hand on control design refinements.

Since sliding effects on the vehicle motion have to be accounted, it would seem natural to rely on vehicle dynamic models. However, the description of dynamic features leads to very large models. Moreover, these models encompass numerous parameters (masses, spring stiffnesses, etc.) whose values are badly known, and very difficult to reach through experimental identification. Finally, some parameters that are of crucial importance (e.g. wheels-ground contact conditions) are even continually varying. Therefore, addressing vehicles control from dynamic models proposes serious difficulties, both from the theoretical and the implementation points of view. Few works (e.g. [5]-[19]) have been reported, but they are concerned with conventional car control on asphalted ground, and moreover, their aim is to prevent the vehicles from sliding. Agricultural context is more involved: the vehicles necessarily undergo sliding, since they are moving on irregular slippery ground. In such harsh conditions, vehicle dynamic models do not appear very tractable from the control design point of view. Therefore, it is proposed here to still rely on standard vehicle kinematic models, derived under pure rolling and non-sliding conditions at wheels-ground contact points, and to account for sliding effects by introducing an additive structured perturbation. Experiments reported here display that these much more compact models, named here below *extended kinematic models*, can nevertheless accurately account for sliding effects on vehicle motion.

This vehicle modeling provides with the very attractive feature that control objective can be addressed, by still relying on powerful guidance laws that can be designed when it is assumed that the vehicles do not slide, while sliding effects can be accounted by introducing adaptive control techniques. More precisely, it is shown here that accurate curved path following can be achieved, by relying on non-linear control laws inferred, under non-sliding assumption, from *Chained Systems Theory* (e.g. [17]), and then extended according to *Internal Model Adaptive* techniques (e.g. [2]-[11]) in order to account for sliding effects. The only unsatisfactory situations are when sliding conditions present large variations (e.g. at the beginning/end of a curve): transient guidance errors can then be observed, due to the delays enclosed in the guidance feedback loop (originating mostly from actuator features). It is however shown here that, by introducing *Model Predictive Control* techniques (e.g.

[14]-[15]) into vehicles guidance laws, guidance accuracy can also be preserved in such situations. Relevancy of this overall control scheme is supported by numerous satisfactory experimental results.

This chapter is organized as follows: first, the experimental context is introduced in Section 2. Then, the proposed vehicle modeling is described in Section 3. Next, guidance laws design is detailed in Section 4. Finally, capabilities of both vehicle modeling and vehicle guidance laws are discussed, relying on numerous experimental reports, in Section 5.

2 Experimental Context

All the vehicle guidance laws designed in the forthcoming Section 4 have been implemented on a full-scale vehicle, and their capabilities have always been extensively investigated via numerous experiments. The more significant experimental results are reported in Section 5.

More precisely, experiments have been performed on a *commercial ARES 640 Renault-Agriculture* farm tractor, lent by *CLAAS*, since this research work has been carried out in partnership with this German agricultural vehicles manufacturer.



Figure 1: ARES 640 farm tractor

The main technical features of this tractor, shown on Figure 1, are given in Table 1. No technical modification has been achieved on this commercial farm tractor, excepted the addition of a *Danfoss* electro-hydraulic valve that enables the automatic steering of the front wheels. The features of this actuator are more detailed in forthcoming Section 4.3, since it will be shown that they have to be accounted in the control law design in order that guidance tasks could be achieved with a satisfactory accuracy. It can also be mentioned that in the addressed guidance applications, the tractor velocity is never automatically controlled. Therefore no specific actuator has been introduced: in all experiments, the tractor velocity is adjusted manually by the farmer.

The tractor localization is achieved relying on an RTK GPS device manufactured by *Thales-Navigation*. More precisely, it is a dual frequency "*Aquarius5002*" unit. When po-

Table 1: ARES 640 main technical features

<u>Dimensions:</u>		<u>Performances:</u>	
Length:	5.2 m	Maximum velocity:	37.5 km.h ⁻¹
Wheelbase:	2.75 m	Working velocity:	8-10 km.h ⁻¹
Height:	2.95 m	Horsepower:	130 CV
	<u>Weight:</u>	Maximum Torque:	54.5 daN.m
without implement:	6370 Kg		

sition measurements are delivered with the upper sampling frequency $f_s = 10 \text{ Hz}$, as it will be in all forthcoming experiments, the claimed accuracy is 2 centimeters. A 1 centimeter accuracy could even be obtained with this unit, but only with a 1 Hz sampling frequency, which is inconsistent with vehicle guidance applications.



(a) Tractor GPS antenna

(b) Base GPS station

Figure 2: RTK GPS equipment

RTK GPS equipment is shown on Figures 2. The tractor GPS antenna, shown on Figure 2(a) is located on the top of the tractor cabin, straight up above the center of the rear axle. This last requirement, as it will be detailed in forthcoming Section 3.4.1, is crucial in order to provide vehicle guidance laws with exactly the position measurements that are expected. Moreover, this position is also consistent with the technological requirements: the top of the tractor cabin is the highest part of the vehicle, and therefore the most convenient place to see as many satellites as possible. The GPS sensor on-boarded on the tractor receives also, via UHF link, the correction information provided online by the GPS base station, depicted on Figure 2(b). This GPS antenna is located accurately at a point whose absolute position is perfectly known, in order that corrections as accurate as possible can be sent. The quality of these corrections is crucial to enable the mobile GPS receiver to deliver the tractor position measurements with the expected 2 cm accuracy.

The on-boarded control device consists in a Pentium based computer. The vehicle position measurements, supplied by the GPS unit, are received via a first RS232 link. They are proceeded by the vehicle guidance laws, implemented in C++ language. The computed steering angle value is then sent to the steering actuator via a second RS232 link. The

farmer can communicate with this control device, or simply supervise the accuracy of the running guidance task, via a Graphical User Interface, shown on Figure 3.

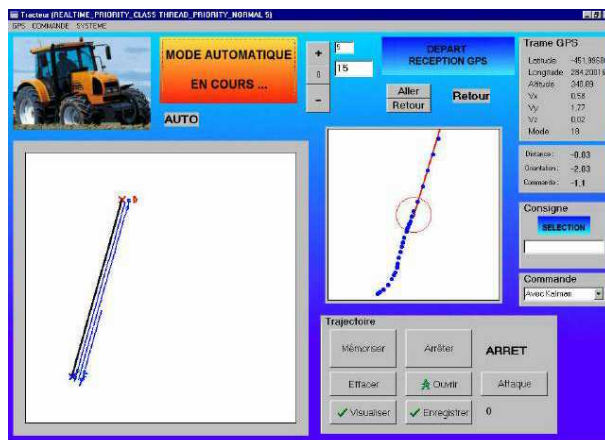


Figure 3: On-boarded Graphical User Interface

3 Vehicle Modeling

The aim of this section is to derive a farm tractor model from which control laws achieving accurate guidance could conveniently be designed. In system modeling, a compromise is generally faced between:

- on one hand, a model which finely describes system behavior, but whose complexity forbids control law design,
- on the other hand, a very simple model, easy to manage from a control design point of view, but which imperfectly accounts for system behavior.

When considering agricultural vehicles, dynamic models appear untractable from a control design point of view. Therefore, as it has been mentioned in the *Introduction*, tractor guidance laws are here designed from a kinematic model, that has been extended in order to account for the main dynamic effects in agricultural applications, namely sliding effects.

More precisely, this section is organized as follows: modeling assumptions and notations are first presented in Section 3.1. Next, the derivation of a vehicle kinematic model under standard non-sliding assumptions is recalled in Section 3.2. Extension of this kinematic model, in order to account for sliding, is then presented in Section 3.3. Finally, measurement and/or estimation of the vehicle state variables is discussed in Section 3.4.

3.1 Modeling Assumptions and Notations

The farm tractor and its possible implement are assumed to constitute a single rigid body (this is the case e.g. with seeders, sprayers, . . .). They are here described according to a

bicycle model (also named *Ackermann's model*): front and rear axles are both replaced by single virtual wheels, located at mid-distance between the actual wheels, see Figure 4. This assumption is quite common in mobile robots literature as long as the vehicles do not slide, see for instance [21]. Its relevancy, when control design is addressed, has been established a posteriori by numerous satisfactory experimental reports. Experiments reported in forthcoming Section 5 show that it is still relevant in presence of sliding, when sliding effects are accounted as a structured perturbation into the vehicle kinematic model.

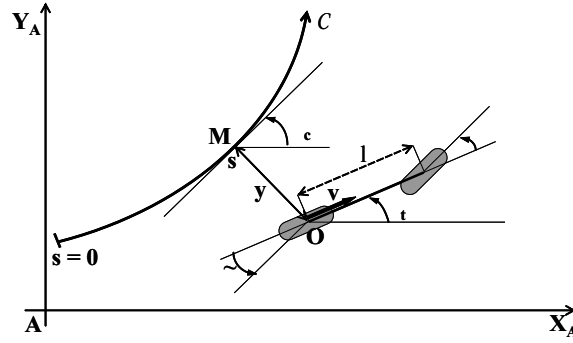


Figure 4: Vehicle description

Since the control objective is path following, the vehicle configuration is here described with respect to the reference path \mathcal{C} , rather than with respect to an absolute reference frame. More precisely, the notations are, see also Figure 4:

- \mathcal{C} is the path to be followed. It is defined in an absolute frame $[A, X_A, Y_A]$,
- O is the center of the vehicle virtual rear wheel (i.e. the center of the tractor rear axle),
- M is the point on \mathcal{C} which is the closest to O . M is assumed to be unique. In practical situations, this assumption is satisfied since, on one hand the tractor remains always close to \mathcal{C} , and on the other hand the curvature of path \mathcal{C} is small.
- s is the curvilinear abscissa of point M along \mathcal{C} , $c(s)$ denotes the curvature of path \mathcal{C} at that point, and $\theta_c(s)$ stands for the orientation of the tangent to \mathcal{C} at that point, with respect to frame $[A, X_A, Y_A]$,
- θ_t is the orientation of the tractor centerline with respect to frame $[A, X_A, Y_A]$. Therefore $\tilde{\theta} = \theta_t - \theta_c(s)$ denotes the angular deviation of the tractor with respect to path \mathcal{C} .
- y is the lateral deviation of the tractor with respect to \mathcal{C} ,
- v is the tractor linear velocity at point O ,
- δ is the orientation of the front wheel with respect to tractor centerline,

- l is the tractor wheelbase.

Since the farm tractor and its possible implement are considered as a single rigid body, the vehicle configuration is described without ambiguity when the location of any point of the vehicle, for instance O , and vehicle centerline orientation are both given. Relying on above notations, these two information can respectively be represented by the couple (s, y) and the variable $\tilde{\theta}$. Vehicle *state vector* can then be written as:

$$X = (s, y, \tilde{\theta})^T \quad (1)$$

Finally, since a kinematic model is here investigated, vehicle *control vector* is:

$$U = (v, \delta)^T \quad (2)$$

Vehicle state space model is now derived, considering successively two possible wheels-ground contact conditions.

3.2 Vehicle Modeling under Non-sliding Assumption

In this section, standard pure rolling and non-sliding contact conditions are assumed to be satisfied. They imply that the linear velocity vector at each wheel center belongs to the wheel plane. When applied to the bicycle model shown on Figure 4, one can obtain that the linear velocity vector at the virtual front wheel center presents an angle δ with respect to the vehicle centerline, and the linear velocity vector at the virtual rear wheel center O , previously denoted v , is directed along the vehicle centerline.

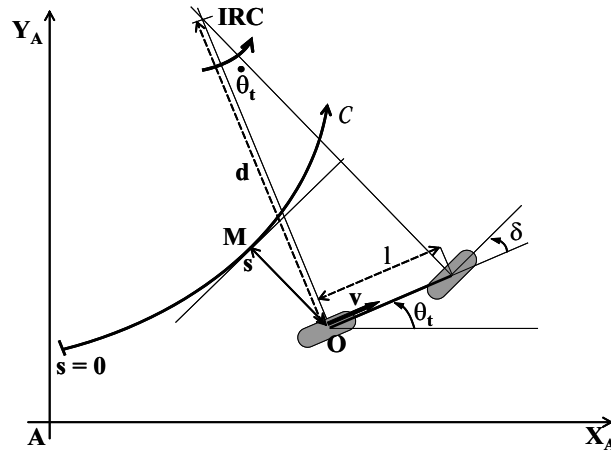
Now, just remind that the vehicle is considered as a rigid body. This ensures that, at each instant, its motion is either a pure translation, or a pure rotation around a moving point termed *Instantaneous Rotation Center (IRC)*. Actually, both situations can be gathered into only one, since translations are just special rotations for which the IRC has moved to infinity. This IRC is clearly defined as the intersection point of the perpendiculars to the linear velocity vectors at any 2 points of the rigid body. This is obvious in the pure rotation case. In the pure translation case, the linear velocity vectors are parallel, the intersection point of their perpendiculars is then consistently rejected to infinity.

On Figure 5, the IRC location is drawn from the perpendiculars to the linear velocity vectors at point O and at the front wheel center, whose directions have been pointed out in the above paragraph. Let us finally denote d , the distance between the IRC and O . The vehicle absolute angular velocity $\dot{\theta}_t$ can then easily be derived: relying on the celebrated relation between angular and linear velocities, it can be obtained that (see Figure 5):

$$\dot{\theta}_t = \frac{v}{d} \quad (3)$$

The value of d can be easily inferred from basic geometrical relations:

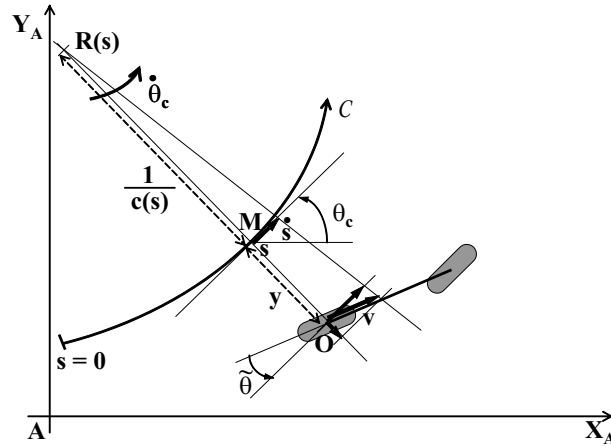
$$\tan \delta = \frac{l}{d} \quad (4)$$

Figure 5: Derivation of the $\dot{\theta}_t$ angular velocity equation

Therefore, gathering (3) with (4) provides us finally with:

$$\dot{\theta}_t = \frac{v}{l} \tan \delta \quad (5)$$

Let us now address the derivation of $\dot{\theta}_c$, relying on Figure 6, where $R(s)$ denotes the curvature center of path C at the curvilinear coordinate s .

Figure 6: Derivation of the $\dot{\theta}_c$ angular velocity equation

By definition, the distance between $R(s)$ and M is $\frac{1}{c(s)}$. Using again the relation between angular and linear velocities, it follows that (see Figure 6):

$$\dot{\theta}_c = \frac{\dot{s}}{\frac{1}{c(s)}} = \frac{v \cos \tilde{\theta}}{\frac{1}{c(s)} - y} \quad (6)$$

Note that y is negative on Figure 6. This explains the minus sign in equation (6). It can be deduced immediately from this latter relation that:

$$\dot{s} = \frac{v \cos \tilde{\theta}}{1 - y c(s)} \quad (7)$$

$$\dot{\theta}_c = \frac{c(s) v \cos \tilde{\theta}}{1 - y c(s)} \quad (8)$$

It is also immediate from Figure 6 that:

$$\dot{y} = v \sin \tilde{\theta} \quad (9)$$

Note that $\tilde{\theta}$ is negative on Figure 6. Signs are then consistent in equation (9). Gathering relations (5), (7), (8) and (9) provides us finally with the *vehicle kinematic model when wheels-ground contact conditions satisfy pure rolling and non-sliding assumptions*:

$$\begin{cases} \dot{s} = v \frac{\cos \tilde{\theta}}{1 - y c(s)} \\ \dot{y} = v \sin \tilde{\theta} \\ \dot{\tilde{\theta}} = v \left(\frac{\tan \delta}{l} - \frac{c(s) \cos \tilde{\theta}}{1 - y c(s)} \right) \end{cases} \quad (10)$$

It can be noticed, that Model (10) becomes singular when $y = \frac{1}{c(s)}$, i.e. when points O and $R(s)$ are superposed. This problem is not encountered in practical situations: on one hand, path curvatures are always small, and on the other hand, it is expected that the farm tractor remains close to \mathcal{C} .

3.3 Vehicle Modeling Accounting for Sliding Effects

In order to account for sliding effects, that inevitably occur in agricultural applications, one possibility is to extend standard kinematic Model (10) with an additive structured perturbation. Such an approach has already been satisfactorily applied to nautical applications, in order to account for stream effects on vessels motion, see [7] and [10]. Since stream acts on vessels in a similar way than sliding acts on land vehicles, this approach is here below investigated.

Let us again describe the farm tractor according to a bicycle model. When sliding occurs, the ground reaction is no longer equal to the wheel action on the ground. The resultant forces at both wheel-ground contact points can be decomposed into longitudinal forces, directed along the wheels planes, and lateral forces, perpendicular to these planes. However, since only lateral guidance applications are here addressed (i.e. the control objective is that the vehicles follow reference paths with a high accuracy), longitudinal sliding resultant forces can be disregarded: first, these forces preponderantly influence the vehicle velocity, whose control is not addressed in path following applications (v is a free control variable, to be tuned by the farmer). Moreover, the performances of lateral guidance laws are shown in

forthcoming Section 4 to be independent from the vehicle velocity. Therefore longitudinal sliding forces have actually a very weak impact in lateral guidance applications, contrarily to lateral sliding forces, denoted \vec{F}_{front} and \vec{F}_{rear} in Figure 7.

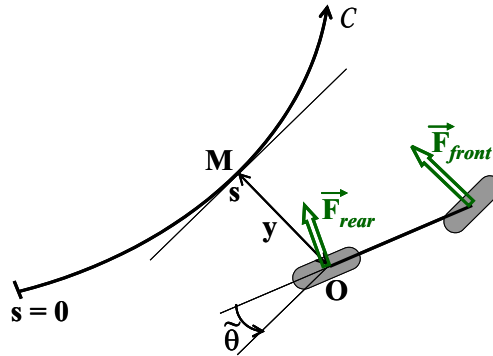


Figure 7: Lateral sliding resultant forces

These two forces obviously generate:

- *a lateral resultant force*, since the projection of \vec{F}_{front} and \vec{F}_{rear} on straight line (MO) is non-null. This leads the vehicle to move sideways.
- *a resultant torque*, since \vec{F}_{front} and \vec{F}_{rear} are generally not identical (due to mass distribution, tire structure, contact conditions at wheel-ground contact points, etc.). This leads the vehicle to turn on itself.

These effects, deduced from schematic Figure 7, can however be also exhibited via thorough vehicle dynamic analysis, see e.g. [4].

Therefore, a *vehicle kinematic model accounting for sliding effects* can be derived by introducing into standard vehicle Model (10) an additive structured perturbation, constituted of a linear lateral velocity \dot{Y}_p and an angular one $\dot{\Theta}_p$:

$$\begin{cases} \dot{s} &= v \frac{\cos \tilde{\theta}}{1-y c(s)} \\ \dot{y} &= v \sin \tilde{\theta} + \dot{Y}_p \\ \dot{\tilde{\theta}} &= v \left(\frac{\tan \delta}{L} - \frac{c(s) \cos \tilde{\theta}}{1-c(s)y} \right) + \dot{\Theta}_p \end{cases} \quad (11)$$

The capabilities of *extended kinematic Model* (11) in describing the vehicle motion in the presence of sliding are demonstrated via full-scale experiments reported in forthcoming Section 5. For the sake of shortening further expressions, the vehicle sliding variables are denoted P in the sequel:

$$P = (\dot{Y}_p, \dot{\Theta}_p)^T \quad (12)$$

3.4 Measurement and Estimation of Vehicle Variables

In order that guidance law design could rely on Model (11), all vehicle variables, namely state vector X and perturbation vector P , have to be available online. As it has been described in Section 2, the only exteroceptive sensor embarked on the farm tractor is an RTK GPS. Direct measurement and/or estimation of vehicle variables from the information supplied by this single sensor are discussed here below.

3.4.1 Direct Measurement of the Vehicle Location

Capabilities of RTK GPS sensor have been presented in Section 2: this sensor can supply the absolute position of its antenna center with a 2 cm accuracy at a 10 Hz frequency.

The GPS antenna has been located on the top of the tractor cabin, accurately straight up above the point O , see Figure 4. Therefore, if the tractor roll and pitch are zero, the absolute position of point O is available by direct measurement. From the knowledge of reference path \mathcal{C} , the location of point M can then easily be inferred. This allows us to have access to the two first coordinates of the tractor state vector: when the tractor roll and pitch are zero, s and y are available online with the same high accuracy than the sensor one.

Since the farm tractors move on irregular ground, roll and pitch are not actually zero. However, in most encountered situations, these two angles present quite small values. Therefore, accuracy of s and y direct measurement is slightly less than the sensor one, but is still satisfactory in order to address accurate automatic guidance applications.

3.4.2 Reconstruction of the Vehicle Heading

When pure rolling and non-sliding conditions are satisfied at wheels-ground contact points, the vehicle linear velocity at point O is directed along the vehicle centerline, as previously mentioned in Section 3.2. Therefore, if reliable velocity measurements were available, the farm tractor heading θ_t could be obtained straightforwardly: let (v_{x_A}, v_{y_A}) denote the coordinates of the linear velocity vector v in the absolute frame $[A, X_A, Y_A]$. Then, θ_t could be computed online according to (see also Figure 4):

$$\theta_t = \begin{cases} \arctan \frac{v_{y_A}}{v_{x_A}} & \text{if } v_{x_A} \neq 0, \\ \text{sign}(v_{y_A}) \frac{\pi}{2} & \text{if } v_{x_A} = 0 \end{cases} \quad (13)$$

Moreover, since the current value of s is already online available (see above), the desired vehicle heading $\theta_c(s)$ can be inferred from the knowledge of reference path \mathcal{C} . Therefore, from a theoretical point of view, the last coordinate of the tractor state vector, namely $\tilde{\theta} = \theta_t - \theta_c(s)$, can then also be obtained online, via direct measurements.

As above mentioned, when the tractor roll and pitch are zero, the single RTK GPS sensor provides us online with the accurate absolute position of point O . The coordinates of velocity vector v can then clearly be inferred, by simply differentiating two successive position information. However, such measurements cannot provide us with accurate enough

values of θ_t . In order to illustrate that point, let us consider a farm tractor describing a perfect straight line (i.e. δ is constantly equal to 0) at 8 km.h^{-1} . The vehicle actual positions at two successive sample times ($T_s = 100 \text{ ms}$, in view of the GPS sensor sampling frequency) are depicted on Figure 8. When the tractor roll and pitch are zero, the vehicle positions provided by the GPS sensor, in view of its accuracy, are inside a 2 cm radius circle centered on the actual point O position. Therefore in the worst case, the vehicle heading computed from (13) could be $\text{atan}(4/22) = 10.3^\circ$ instead of a null expected heading, as shown on Figure 8. This theoretical maximum heading measurement error is of course larger if the vehicle velocity is smaller. Moreover, if the tractor roll and pitch are not zero and/or the vehicle undergoes sliding, the accuracy of vehicle heading direct measurement may still be significantly damaged.

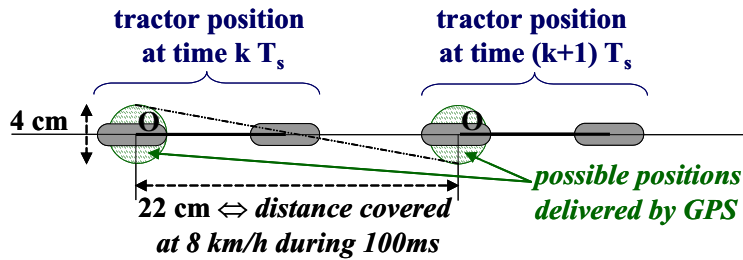


Figure 8: Theoretical computation of the accuracy of the heading direct measurement

Straight line runs at 8 km.h^{-1} have been performed with our experimental set up, in order to investigate whether the theoretical maximum heading measurement error computed above is representative for actual applications or not. Experimental data reveal that θ_t maximum value provided by relation (13) is 11.81° (instead of a null expected heading) and that the standard deviation of θ_t values is 2.4° . These experimental data are therefore consistent with theoretical computations depicted on Figure 8.

If θ_t direct measurements were used straightforwardly inside automatic guidance law (designed in forthcoming Section 4), computed steering angle δ would clearly be very oscillating. Depending on the actuator bandwidth, these oscillations could either be transmitted to the front wheels or be filtered out. In the latter situation, which is however not at all a very satisfactory one, the oscillations in θ_t direct measurements would not be perceptible on the vehicle motion. In order to settle this point, spectral analysis has been carried out on experimental data recorded in the above mentioned experiments. The spectral modes of θ_t signal provided by direct measurements (i.e. computed from RTK GPS information and relation (13)) are shown in dash-dotted line on Figure 9. During these experiments, a vehicle heading measurement device (consisting in a double GPS antenna) had also exceptionally been embarked on the tractor, in order to provide with more reliable θ_t values. The spectral modes of this latter signal are shown in dashed line on Figure 9.

It can be observed on Figure 9 that the θ_t signal delivered by a single RTK GPS according to (13) displays very low frequency modes (0.3 Hz , 1 Hz , \dots). These modes could definitely not be filtered out by the steering actuator, since its bandwidth can be shown to

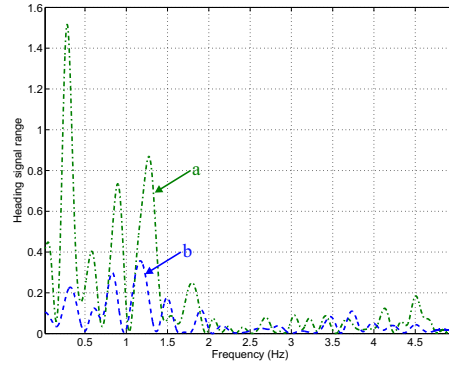


Figure 9: Spectral analysis of θ_t direct measurement (dash-dotted - *a*) and θ_t provided by a double GPS antenna (dashed - *b*)

be close to 2 Hz, see forthcoming Section 4.3. With a much lower order of magnitude, the same low frequency modes are observed on the θ_t signal delivered by the double GPS antenna device. Therefore, it appears that the oscillations in the θ_t signal delivered by a single RTK GPS originate from perturbations such as the tractor roll and pitch and/or sliding effects, and then are amplified since velocity measurements cannot be provided with a sufficient accuracy, as highlighted on Figure 8.

The spectral analysis depicted on Figure 9 demonstrates that, if automatic guidance is intended to be achieved relying solely on a RTK GPS sensor, then the vehicle heading θ_t must be filtered prior to be sent to the steering law. Since tractor models are available, an efficient alternative to standard digital filters consists in making use of them through a *Kalman state reconstructor*.

Let us assume again that pure rolling and non-sliding conditions are satisfied at wheels-ground contact points. Then, θ_t equation is given by (5). Since v and δ are both control variables, this equation is a priori a non-linear one. However:

- on one hand, for obvious practical reasons, δ is bounded:

$$|\delta| < \delta_{max} < \frac{\pi}{2}$$

Therefore, $\tan \delta$ can be regarded as a control variable in the place of δ .

- on the other hand, since the control objective in forthcoming Section 4 is to achieve path following, v is not actually regarded as a control variable: it is a free parameter to be tuned by the farmer, whose value may possibly be slowly varying.

In view of these two remarks, equation (5) can actually be considered as a linear equation, and celebrated Kalman linear state reconstructor can be used. More precisely, discrete analogue of equation (5) is:

$$\theta_{t,[k]} = \theta_{t,[k-1]} + \frac{v T_s}{l} \tan \delta_{[k-1]} \quad (14)$$

where T_s is the sampling period. The model and the innovation equations of the Kalman state reconstructor associated with Model (14) are, see e.g. [6]:

$$\begin{cases} \bar{\theta}_{t,[k]} &= \hat{\theta}_{t,[k-1]} + \frac{v T_s}{l} \tan \delta_{[k-1]} \\ \hat{\theta}_{t,[k]} &= \bar{\theta}_{t,[k]} + L (\theta_{t,[k]} - \bar{\theta}_{t,[k]}) \end{cases} \quad (15)$$

$\theta_{t,[k]}$ is the k^{th} sample of the raw vehicle heading θ_t , derived from the velocity measurements supplied by the RTK GPS and relation (13). $\bar{\theta}_{t,[k]}$ is the k^{th} prediction of signal θ_t , and $\hat{\theta}_{t,[k]}$ is the k^{th} sample of the filtered heading signal, that will be used in the forthcoming guidance laws. Finally, L is the scalar Kalman gain, to be chosen with respect to the RTK GPS sensor features. In all forthcoming experiments, L has been tuned to 0.08.

The capabilities provided by heading reconstructor (15) have been investigated via two sets of experiments.

First, straight line runs have again been performed. The vehicle heading θ_t , which is expected to be constantly zero, has been computed from the velocity measurements supplied by the RTK GPS and relation (13), and then filtered according to (15). Filtering benefits appear clearly in Table 2:

Table 2: θ_t measurement / reconstruction during straight line runs

	max. value	standard deviation
θ_t computed directly from (13)	11.81°	2.4°
θ_t computed from reconstructor (15)	3.61°	0.86°

In view of Table 2, in a steady state (i.e. when the vehicles describe straight lines), accuracy of the vehicle heading θ_t provided by Kalman reconstructor (15) appears satisfactory and consistent with path following applications.

The capabilities of reconstructor (15) when the vehicle heading is varying, and especially the delay introduced by that filter, have been investigated via a second set of experiments: the farm tractor has been manually driven in order to describe successively a straight line, then the quarter of a circle, and finally a straight line. The vehicle heading θ_t , either computed directly from the velocity measurements provided by the RTK GPS and relation (13), or proceeded through Kalman reconstructor (15), is displayed on Figure 10 respectively in dash-dotted and solid lines. These signals are compared with the signal supplied by a reliable heading measurement device (namely a double GPS antenna) shown in dashed line on Figure 10.

It can be seen on Figure 10 that the vehicle heading θ_t , when computed directly from the velocity measurements supplied by the RTK GPS and relation (13), is a very noisy signal. This negative feature is even more important when the vehicle heading is varying, see the zoom shown on Figure 10. The guidance laws to be designed in forthcoming Section 4 cannot clearly rely on a so noisy heading information. In contrast, it can be observed on Figure 10 that the vehicle heading θ_t provided by Kalman reconstructor (15) follows very

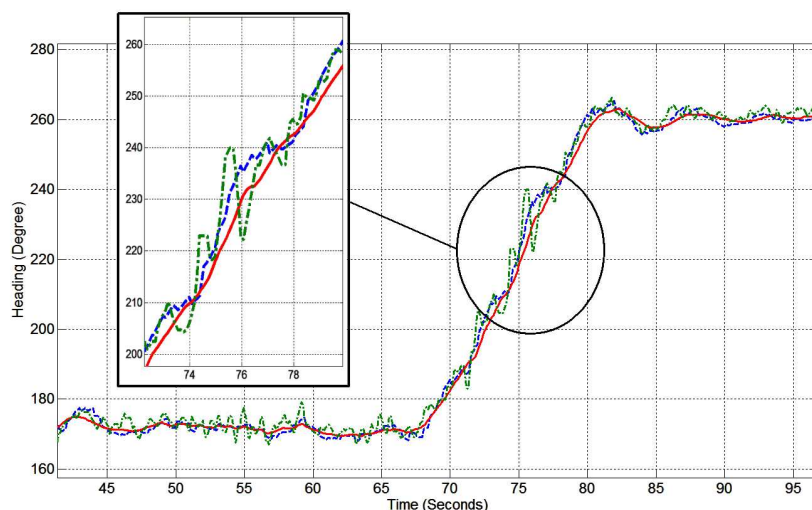


Figure 10: Vehicle heading θ_t signals. *Dashed line*: double GPS antenna, *dash-dotted line*: computed directly from (13), *solid line*: obtained from reconstructor (15)

closely the reliable vehicle heading supplied by the double GPS antenna. More precisely, it can be noticed that:

- as expected, the vehicle heading θ_t proceeded through Kalman reconstructor is no longer a noisy signal,
- moreover, reconstructor equations (15) have been derived under assumptions of pure rolling and non-sliding conditions at wheels-ground contact points. When the farm tractor enters into the circular part of its path, these assumptions are no longer satisfied: sliding necessarily occurs. Nevertheless, the vehicle heading θ_t derived from equations (15) still fits quite satisfactorily with the actual vehicle heading supplied by the double GPS antenna.
- the delay introduced by the Kalman reconstructor, even when sliding occurs, never climbs over 300 ms, see the zoom shown on Figure 10. This is not prohibitive with respect to the considered applications (heavy farm tractors cannot change significantly their heading in a so short time).

Therefore, embarking an additional heading measurement device (such as a double GPS antenna) does not appear mandatory in order to achieve path following. In all guidance experiments reported in forthcoming Section 5, the vehicle heading will be provided from the information supplied by the single RTK GPS sensor, and proceeded through Kalman reconstructor (15).

3.4.3 Estimation of the Sliding Variables

As shown above, the single RTK GPS sensor can provide online with the whole vehicle state vector X . Therefore, it enables to achieve path following, as long as sliding effects have not to be accounted. Such path following control laws, relying on Model (10) (i.e. model without sliding), are designed in Section 4.1, and related full-scale experiments are reported in Section 5.1. As expected, satisfactory guidance accuracy is displayed as long as the vehicles do not enter into sharp curves or move on sloping fields. In these two latter situations, sliding occurs and decreases guidance accuracy.

In order to preserve the guidance accuracy in these situations, sliding effects have to be accounted explicitly in control laws. This imposes that perturbation vector P must also be available online. A direct measurement would require sophisticated devices, and their accuracies would not be guaranteed on irregular agricultural fields. Therefore, it is proposed here to still rely on the single RTK GPS sensor, and to estimate P according to an *Internal Model Adaptive scheme*.

More precisely, at each sample time, the RTK GPS sensor provides with the actual vehicle behavior, assumed to obey Model (11). Perturbation vector P can then be derived by comparing this actual behavior to the theoretical behavior in the absence of sliding, which can be obtained by simulating Model (10) with the actual steering angle δ applied to the vehicle. This estimation scheme is depicted on Figure 11.

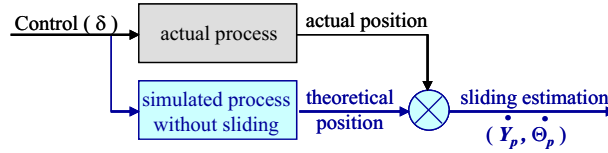


Figure 11: Sliding variables estimation scheme

Explicit estimation equations can be derived from Models (10)-(11) and relation (5):

$$\begin{cases} \dot{Y}_{P,[k]} &= \frac{y_{[k]} - y_{[k-1]}}{T_s} - v \sin \tilde{\theta}_{[k-1]} \\ \dot{\Theta}_{P,[k]} &= \frac{\theta_{t,[k]} - \theta_{t,[k-1]}}{T_s} - v \frac{\tan \delta_{[k-1]}}{L} \end{cases} \quad (16)$$

As usual, T_s denotes the sampling period and subscripts $_{[k]}$ refer to the k^{th} sample. It is worth noticing that perturbation vector P is not computed from absolute lateral and angular deviations, but more conveniently from relative deviations occurring during a sampling period. Sliding estimation algorithm is therefore independent from vehicle absolute deviation.

It is clear from equations (16) that perturbation vector P does not account specifically for sliding effects: any perturbation acting on standard Model (10) in a similar way than sliding effects (i.e. by introducing additional lateral and angular velocities) is also accounted. Therefore, the values presented by perturbation vector P are mainly explained by sliding occurrence, but other dynamic effects may also be superposed inside P : delays

originating from vehicle large inertia, oscillations due to vehicle roll and pitch, etc. The aggregation of the perturbations acting on the vehicle exhibits positive and negative features:

- positive feature: in forthcoming Section 4.2, vehicle guidance laws are modified, according to adaptive control techniques, in order to annihilate the impact of perturbation vector P on guidance accuracy. The main objective of this adaptive control design is to preserve guidance accuracy when the vehicles undergo sliding. However, the same positive action is obtained with respect to any other perturbation accounted in P . Therefore, vehicle guidance accuracy is finally also improved with respect to some other dynamic phenomena that had not been explicitly considered when designing Model (11) (such as e.g. delays originating from the vehicle large inertia).
- negative feature: since perturbation vector P does not specifically describe sliding effects and some well-identified dynamic phenomena, it will be a quite noisy signal. For instance, due to ground irregularities, the tractor cabin undergoes necessarily some roll. Since the GPS antenna is located on the cabin, roll alters lateral deviation measurements and, in view of equations (16), roll is finally incorporated into perturbation vector P , despite it has no effect on point O location. Moreover, since measurement data are somehow differentiated in estimation equations (16), these parasitic phenomena could be significantly amplified.

Therefore, perturbation vector P must be filtered in order to preserve the useful information and, at minimum, be accurately representative for sliding effects, as desired. Since no model is available for parasitic phenomena, standard digital filters have been investigated: more precisely, a first order Butterworth low-pass filter has been considered, in order to avoid the introduction of too much delay in sliding estimation.

The capabilities of Model (11) and estimation algorithm (16) to account for sliding effects in the vehicle motion have been investigated via full-scale experiments. Satisfactory results, recorded when the farm tractor describes sharp curves on a level ground, or when it describes straight lines on a sloping field, are reported and discussed in forthcoming Section 5. Control law design, relying on Model (11), is now addressed in the next Section, with the aim to achieve accurate path following, even when the vehicles undergo sliding.

4 Path Following Control Law Design

The control objective is to provide farm vehicles with accurate path following capabilities. The reference path is known: it has either been computed from a GPS map of the field, or been experimentally learnt (i.e. the farm tractor is manually driven along the desired reference path, and this latter is then recorded from the tractor RTK GPS sensor).

Vehicle modeling presented in Section 3 is very suitable to address this problem, since the control objective can be expressed very simply as "*bringing and keeping lateral deviation y to 0*". When the vehicles do not undergo sliding, angular deviation $\tilde{\theta}$ is also expected to converge to 0 (this intuitive feature can also be recovered from the second equation in

Model (10)). In contrast, when sliding occurs, the convergence of y is no longer consistent with that of $\tilde{\theta}$: it can be derived from the second equation in Model (11) that the asymptotic value of $\tilde{\theta}$ depends on \dot{Y}_P . From a practical point of view, when sliding occurs, the vehicles have to move slightly crabwise in order to ensure a null lateral deviation.

Path following applications are not concerned with vehicle velocity control: v must be a free parameter that can be tuned online by the farmer according to the agricultural task to be achieved. Therefore, with respect to guidance control laws, v has to be considered as a parameter whose value may possibly be slowly varying. The sole available control variable is the steering angle δ .

This section is organized as follows: first, vehicle automatic guidance when sliding does not occur is addressed in Section 4.1. Non-linear control techniques are applied on Model (10), and provide with very satisfactory guidance performances. In order to preserve these performances when sliding occurs, previous guidance laws are refined in Section 4.2, relying on adaptive control techniques applied from Model (11). Guidance performances are shown to be satisfactory excepted at sliding appearance/disappearance. The overshoots that can be observed originate mainly from the delay introduced by the steering actuator. Model predictive control techniques are then investigated in Section 4.3 to cope with this difficulty. Performances of the proposed guidance laws are finally displayed from numerous full-scale experiments reported in forthcoming Section 5.

4.1 Non-linear Control in Absence of Sliding

When sliding effects are not accounted, the vehicle motion is described by Model (10). This model is clearly a non-linear one. In [1], the authors propose to linearize it around the equilibrium $y = \tilde{\theta} = 0$, in order that celebrated Linear Systems theory could be used. In that case, control design does not rely on the actual vehicle model, but on an approximated one. Recent advances in Control theory have established that mobile robots models can be converted into almost linear models, namely *chained forms*, in an exact way, see e.g. [17]. Such an approach is attractive since it allows to use, for a large part, Linear Systems theory, while still relying on the actual non-linear vehicle model. This approach is followed in the sequel.

4.1.1 Conversion of Vehicle Model (10) into Chained Form

The general chained form dedicated to systems with two inputs is written as (see [17]):

$$\left\{ \begin{array}{l} \dot{a}_1 = m_1 \\ \dot{a}_2 = a_3 m_1 \\ \dot{a}_3 = a_4 m_1 \\ \dots \\ \dot{a}_{n-1} = a_n m_1 \\ \dot{a}_n = m_2 \end{array} \right. \quad (17)$$

with $A = (a_1, a_2, \dots, a_n)^T$ and $M = (m_1, m_2)^T$ respectively the state and control vectors. In order to point out that a chained system is almost linear, just replace the time derivative by a derivation with respect to the state variable a_1 . Using the notations:

$$\frac{d}{da_1} a_i = a'_i \quad \text{and} \quad m_3 = \frac{m_2}{m_1} \quad (18)$$

the chained form (17) can be rewritten:

$$\left\{ \begin{array}{l} a'_1 = 1 \\ a'_2 = a_3 \\ a'_3 = a_4 \\ \dots \\ a'_{n-1} = a_n \\ a'_n = m_3 \end{array} \right. \quad (19)$$

The last $n - 1$ equations of system (19) constitute clearly a linear system.

Let us now convert vehicle Model (10) into chained form. When limited to dimension 3, the general chain systems (17) and (19) are written respectively as:

$$\text{derivation w.r. to time : } \left\{ \begin{array}{l} \dot{a}_1 = m_1 \\ \dot{a}_2 = a_3 m_1 \\ \dot{a}_3 = m_2 \end{array} \right. \quad (20)$$

$$\text{derivation w.r. to } a_1 : \left\{ \begin{array}{l} a'_1 = 1 \\ a'_2 = a_3 \\ a'_3 = m_3 \end{array} \right. \quad (21)$$

Since control law performances are expected to be independent from the vehicle velocity, the variable a_1 , which drives the linear system (21), should be homogeneous at the distance covered by the vehicle. A natural choice is then:

$$a_1 = s \quad (22)$$

Straightforward computations show now that the non-linear vehicle Model (10) can actually be converted into chained forms (20) or (21) from the starting choice (22).

In order to fit with (20), the new control m_1 is necessarily defined as:

$$m_1 \triangleq \dot{a}_1 = v \frac{\cos \tilde{\theta}}{1 - y c(s)} \quad (23)$$

Moreover, for the sake of simplicity, let us try:

$$a_2 = y$$

It follows that:

$$\dot{a}_2 = v \sin \tilde{\theta} \triangleq a_3 m_1$$

Therefore the last state variable a_3 must be chosen as:

$$a_3 = (1 - y c(s)) \tan \tilde{\theta}$$

Finally, the last control variable m_2 is necessarily given by:

$$\begin{aligned} m_2 \triangleq \dot{a}_3 &= \frac{d}{dt}((1 - y c(s)) \tan \tilde{\theta}) \\ &= -c(s) v \sin \tilde{\theta} \tan \tilde{\theta} - \frac{dc(s)}{ds} \frac{v \cos \tilde{\theta}}{1 - y c(s)} \tan \tilde{\theta} y \\ &\quad + v \frac{(1 - y c(s))}{\cos^2 \tilde{\theta}} \left(\frac{\tan \delta}{l} - c(s) \frac{\cos \tilde{\theta}}{1 - y c(s)} \right) \end{aligned} \quad (24)$$

As a conclusion, the non-linear tractor Model (10) can be converted into chained forms (20) or (21) in an exact way according to the state transformation:

$$A = \Psi(X) \quad \text{with} \quad \Psi(X) = (s, y, (1 - y c(s)) \tan \tilde{\theta})^T \quad (25)$$

and the control transformation:

$$M = \Upsilon(U, X) \quad \text{defined by (23) and (24)} \quad (26)$$

These transformations are invertible as long as $y \neq \frac{1}{c(s)}$ (model singularity), $v \neq 0$, and $\tilde{\theta} \neq \frac{\pi}{2} [\pi]$. From a practical point of view, once properly initialized, the guided vehicle respects these conditions.

4.1.2 Non-linear Control Law Design

Control design can now be completed in a very simple way: since chained form (21) is linear, a natural expression for the virtual control law is:

$$m_3 = -K_d a_3 - K_p a_2 \quad (K_p, K_d) \in \mathcal{R}^{+2} \quad (27)$$

As a matter of fact, injecting (27) into (21) leads to:

$$a_2'' + K_d a_2' + K_p a_2 = 0 \quad (28)$$

which implies that a_2 converges to zero. In view of (25), the convergence of y to 0 is therefore ensured: path following is clearly achieved. Moreover, the convergence of a_2 implies that of a_3 (in view of chained form (21)). State transformation (25) ensures then that angular deviation $\tilde{\theta}$ converges also to 0.

Since the error dynamics (28) is driven by $a_1 = s$, the gains (K_d, K_p) impose a settling distance instead of a settling time. Consequently, for a given initial error, the vehicle trajectory will be identical, whatever the value of v is, and even if v is time-varying. From a control design point of view, guidance performances are velocity independent: control law gains have not to be adjusted with respect to vehicle velocity v . In practical situations,

this theoretical result might be slightly altered, since the quality of θ_t (and therefore of $\tilde{\theta}$) measurement clearly depends on v (relations (13) and (15)), or since the tractor actuators are not perfectly linear. Nevertheless, as long as standard agricultural velocities (from 4 to 14 $km.h^{-1}$) are concerned, and provided that control gains (K_d , K_p) are not so high that actuators are saturating, experimental results demonstrate that guidance performances are actually velocity independent, see forthcoming Section 5.1.

Ultimately, the inversion of control transformations (26) provides with the actual control law expression (just report (27) in (18), (23) and (24)):

$$\delta(y, \tilde{\theta}) = \arctan \left(l \left[\frac{\cos^3 \tilde{\theta}}{(1-yc(s))^2} \left(\frac{dc(s)}{ds} y \tan \tilde{\theta} - K_d (1-yc(s)) \tan \tilde{\theta} - K_p y + c(s) (1-yc(s)) \tan^2 \tilde{\theta} \right) + \frac{c(s) \cos \tilde{\theta}}{1-yc(s)} \right] \right) \quad (29)$$

It is worth noticing that no approximation has been introduced in control design. This enables non-linear control law (29) to ensure accurate curved path following: non-linearities of Model (10) and curvature $c(s)$ of the reference path are both explicitly accounted in control expression. In addition, performances tuning of non-linear control law (29) is still very easy, since it relies on linear error equation (28): a settling distance can very intuitively be imposed by just adjusting gains K_p and K_d . Moreover, since a settling distance instead of a settling time is imposed, guidance law performances are actually independent from the vehicle velocity, even if v is varying.

In many applications, the reference path \mathcal{C} is a straight line, i.e. $c(s) = 0$. The expression of the control law (29) turns then simpler:

$$\delta(y, \tilde{\theta}) = \arctan(l \cos^3 \tilde{\theta} (-K_d \tan \tilde{\theta} - K_p y)) \quad (30)$$

Finally, let us go back to the discussion on actuators saturation. In control laws (29) or (30), the argument of the *arctan* function is not bounded. Therefore actuators saturation can a priori occur. The natural way to deal with it, is to adjust control performances (i.e. to tune gains (K_d , K_p)) in order that saturations are never met during prespecified operations. However, it can be pointed out that actuators saturation does not prevent from the vehicle convergence to the reference path \mathcal{C} , even from a theoretical point of view: since chained form (21) consists in a double integrator, its asymptotic stability is still ensured, even if the virtual control law (27) is bounded to any arbitrary value, see [18]. Unfortunately, in view of (29), the boundedness of m_3 leads to that of δ only if the reference path curvature $c(s)$ exhibits some good properties. However, in most practical situations, these properties are satisfied, so that the theoretical stability is actually preserved. For instance, it is obviously checked when \mathcal{C} is a straight line, since $c(s) = 0$. The only drawback is that control performances are, of course, no longer velocity independent as soon as the actuators are saturating.

Actually, the main difficulty proposed by the steering actuator is not saturations, but the introduction of delays into the guidance feedback loop. The influence of these delays is very perceptible when sliding occurs, as it can be seen on experimental reports in Section 5.2. This actuator feature is accounted in Section 4.3, relying on Model Predictive techniques.

4.2 Internal Model Adaptive Control Accounting for Sliding Effects

Sliding effects are described in Model (11) as an additive structured perturbation. When such additive perturbations are constant or slowly-varying, they can be easily rejected by introducing integral correction terms into control law design. However, in agricultural tasks, sliding is definitely not a static perturbation. In contrast, its dynamics exhibits high frequency modes. Therefore, sliding effects cannot be accounted accurately by simply adding integral correction terms into control law (29). Full-scale experiments have been carried out and have corroborated this conclusion.

Adaptive control techniques propose a more convenient framework to cope with additive structured perturbations. Such an approach has for instance been developed in [3] for a harvesting application relying on a video camera sensor: when sliding effects are detected, a correction term computed from an empirical relation is incorporated into the guidance law previously derived under classical pure rolling and non-sliding contact conditions. Full-scale experiments demonstrate that this adaptive correction scheme improves significantly guidance accuracy in the presence of sliding.

In this Section, *Internal Model adaptive control* techniques, see e.g. [2]-[11], are used to deal with sliding effects. The major advantage of this approach is that it allows to account for sliding while still relying on non-linear control law (29) designed in previous section. Thus, all positive features of this guidance law (accuracy, intuitive performances tuning, performances independent from vehicle velocity, . . .) can be preserved.

As a first step, let us address an academic case where perturbation vector P is constant (for instance, when the vehicle describes a straight line on a field with a perfect constant slope). In such a case, it can be shown that non-linear control law (29), which does not account for sliding effects, leads to asymptotic constant guidance errors. More precisely, from Model (11), it can be obtained immediately that:

$$\tilde{\theta} \xrightarrow{t \rightarrow \infty} -\arcsin\left(\frac{\dot{Y}_p}{v}\right) \quad (31)$$

$$\frac{\tan \delta}{L} \xrightarrow{t \rightarrow \infty} -\frac{\dot{\Theta}_p}{v} + \frac{c(s) \cos \tilde{\theta}}{1 - c(s)y} \quad (32)$$

Then, injecting (32) into (29) shows that:

$$\frac{\cos^3 \tilde{\theta}}{(1 - c(s)y)^2} (\alpha y + \beta) \xrightarrow{t \rightarrow \infty} -\frac{\dot{\Theta}_p}{v} \quad (33)$$

where:

$$\begin{aligned}\alpha &= \frac{dc(s)}{ds} \tan \tilde{\theta} + c(s) \tan \tilde{\theta} (K_d - c(s) \tan \tilde{\theta}) - K_p \\ \beta &= \tan \tilde{\theta} (c(s) \tan \tilde{\theta} - K_d)\end{aligned}$$

Finally, by neglecting second order term y^2 in (33), it can be proved that:

$$y \xrightarrow{t \rightarrow \infty} -\frac{\beta + \frac{\dot{\theta}_p}{v \cos^3 \tilde{\theta}}}{\alpha - \frac{2c(s)\dot{\theta}_p}{v \cos^3 \tilde{\theta}}} \triangleq y_c \quad (34)$$

Provided that reference path curvature $c(s)$ is constant or slowly varying, relations (34) and (31) and finally relation (32) establish that lateral and angular deviations (i.e. y and $\tilde{\theta}$) as well as control variable δ asymptotically converge to constant or slowly varying non-null values. This shows that, in response to constant sliding conditions, non-linear control law (29) leads the vehicles to move crabwise. This is somehow consistent with the behavior that can be observed when the vehicles are manually driven.

In the special case where $c(s)$ is constant, the convergence of lateral deviation y to 0, despite the presence of sliding, can be very simply achieved by just shifting the objective of non-linear control law (29): if the objective of control law (29) (which does not account for sliding) is henceforth to bring y to the constant value $-y_c$, then it is clear that the vehicle actual lateral deviation (which undergoes sliding effects) converges to 0. Guidance accuracy is then preserved, although the vehicle is still moving crabwise (relations (31)-(32) are not affected by the control law modification). The expression of the new control law can be deduced straightforwardly from (29):

$$\begin{aligned}\delta &= \arctan \left(L \left[\frac{\cos^3 \tilde{\theta}}{(1-c(s)(y+y_c))^2} \left(\frac{dc(s)}{ds} (y+y_c) \tan \tilde{\theta} \right. \right. \right. \\ &\quad \left. \left. - K_d(1-c(s)(y+y_c)) \tan \tilde{\theta} - K_p(y+y_c) \right. \right. \\ &\quad \left. \left. + c(s)(1-c(s)(y+y_c)) \tan^2 \tilde{\theta} \right) + \frac{c(s) \cos \tilde{\theta}}{1-c(s)y} \right] \right) \quad (35)\end{aligned}$$

In agricultural tasks, perturbation vector P and path curvature $c(s)$ are obviously not constant. However, if the shift y_c in the control law objective could track the current sliding conditions, then adaptive non-linear control law (35) would still improve guidance accuracy. Two approaches are proposed below to achieve such an online y_c adaptation:

- Model Reference Adaptive Control (MRAC):

MRAC scheme is depicted on Figure 12(a). It consists in a simulation application that is constantly running when the vehicle is moving. The equations that are simulated are Model (11) (i.e. vehicle model accounting for sliding). Simulated steering variable δ is computed from control law (29) (i.e. guidance law without sliding accounted), and components of perturbation vector P used in the simulation are the sliding effects acting on the actual vehicle, provided online by estimation algorithm (16). State variable y of this simulation application is then used as the corrective term y_c to be introduced into the control law (35) that steers the actual vehicle.

When perturbation vector P is constant, the simulated state variable y clearly converges to the theoretical value (34), which is suitable to ensure that control law (35)

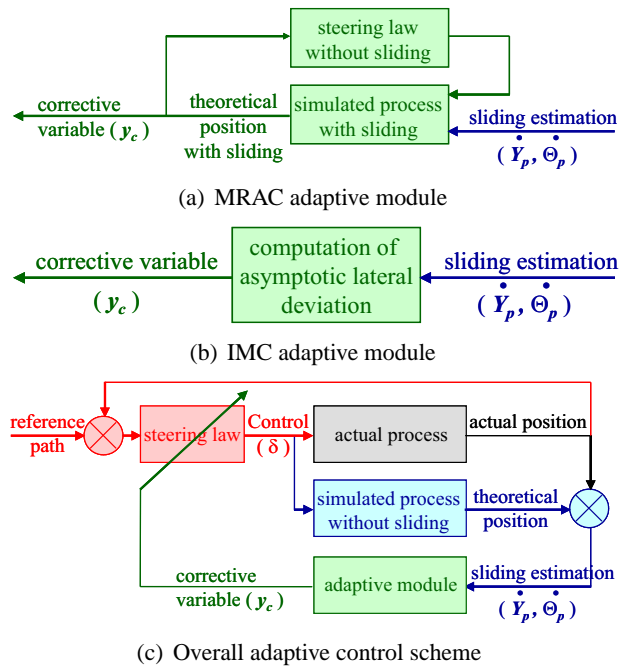


Figure 12: Block-diagrams describing adaptive control scheme

brings the vehicle lateral deviation to 0, despite the presence of sliding. In the general case, where P is varying, the simulated state variable y is only reflecting current sliding conditions. However, its introduction into control law (35) can intuitively improve path following accuracy. This is corroborated by full-scale experiments reported in Section 5.2.

- Internal Model Control (IMC):

IMC scheme is depicted on Figure 12(b). In this second approach, the corrective shift y_c to be introduced into control law (35) is directly computed by injecting the actual sliding conditions provided by online estimation algorithm (16) into relation (34).

When perturbation vector P is constant, the corrective shift y_c is then immediately the suitable one, that can ensure the convergence to 0 of the vehicle lateral deviation. When P is varying, the computed y_c value is also reflecting current sliding conditions, and can also intuitively improve path following accuracy, as corroborated by full-scale experiments reported in Section 5.2.

When perturbation vector P is constant, IMC scheme offers immediately the suitable y_c value. In contrast, this suitable value is not instantaneously available in the MRAC scheme, since one has to wait for the convergence of the simulation application. Therefore, IMC scheme may appear more relevant. However, perturbation vector P delivered by estimation algorithm (16) is a quite noisy signal (as mentioned in Section 3.4.1). In IMC scheme, this noisy feature is entirely propagated to the corrective shift y_c , since it is directly computed

from the values of P (via relation (34)). Therefore, in order to avoid the transmission of high frequency modes to the steering actuator, y_c values computed from IMC scheme have eventually to be filtered. In contrast, MRAC scheme does not propose the same difficulty since the simulation application acts as a natural low-pass filter. Therefore, none of these two approaches appears clearly superior to the other one.

The overall adaptive control scheme is depicted on Figure 12(c), where the adaptive module consists either in MRAC scheme or in IMC scheme. Nevertheless, whatever this adaptive module is, the proposed guidance law fits with standard Internal Model adaptive control scheme.

4.3 Model Predictive Control Accounting for Actuator Features

The steering actuator embarked on the farm tractor, introduced briefly in Section 2, is an electro-hydraulic valve. As already mentioned, the main limitation of that device is that it introduces an undesired delay in the global guidance feedback loop. The influence of that delay is particularly perceptible when the vehicles undergo sliding: as long as sliding conditions are slowly varying, e.g. when the vehicles are describing a curve, control law (35) satisfactorily ensures an accurate path following. In contrast, when sliding conditions are changing, e.g. when the vehicles enter into a curve or exit from a curve, prohibitive transient guidance errors can be observed. The delay in the actuation, if not the sole responsible, is nevertheless the main responsible for such overshoots. Since this delay is not inherent to our steering actuator, but is more or less present in any actuation device, *Model Predictive control* has been investigated with the aim to bring some anticipation to control law (35), in order to significantly reduce these disappointing overshoots. Moreover, when tuning the predictive parameters, it can be accounted in control law (35), not only for actuation delay, but also for some other dynamic phenomena, such as the vehicle large inertia.

4.3.1 Identification of Steering Actuator Model

In order to support predictive control design, a model describing actuator behavior must be available. This actuator consists in an electro-hydraulic valve controlled via an inner closed-loop scheme, as depicted on Figure 13. The actual front wheel angle δ_a is measured via an absolute encoder and compared with the desired one, denoted δ_d , provided by the guidance law (i.e. control law (29) or (35)). A Proportional-Derivative algorithm, implemented on a PCB80C552 microprocessor, controls then the voltage u applied between the two electrical wires of the valve, in order to adjust the oil flow p such that the front wheels angle δ_a fits at best with δ_d .

In order to derive the actuator model, several step inputs in desired steering angle δ_d have been applied. The actual steering angle δ_a has then been recorded. It can be obtained from these experiments that the actuation device presents:

- perfect steady state capabilities: the steady state error between δ_d and δ_a is less than 0.1° ,

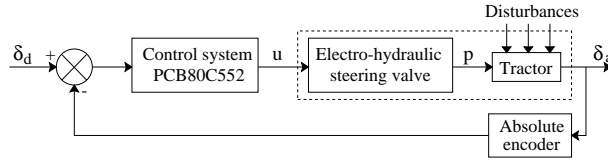


Figure 13: Block-diagram of the steering actuator

- a 600 *ms* rise time (by the way, this establishes that the actuator bandwidth, questioned in Section 3.4, is actually close to 2 *Hz*)
- a 10% overshoot in step responses.

The 600 *ms* rise time cannot be reduced since it is inherent to the actuator technology, and more precisely to the hydraulic pump capabilities: at tractor nominal engine speed, i.e. 2000 *tr.mn*⁻¹, the maximum oil flow *p* delivered by the hydraulic pump is limited to 25 *l.mn*⁻¹. At low engine speed (never used in forthcoming experiments), the maximum value of *p* would even fall to 12 *l.mn*⁻¹, which would still increase inner closed-loop delays.

Relying on these experimental step responses, standard identification techniques establish that this steering actuator can be satisfactorily described by a linear second order model. Its discrete transfert function, to be used in forthcoming predictive control design, is given by:

$$F(z^{-1}) = \frac{\delta_a(z^{-1})}{\delta_d(z^{-1})} = \frac{0.1237 z^{-1} + 0.0934 z^{-2}}{1 - 1.2155 z^{-1} + 0.4326 z^{-2}} \quad \left(\begin{array}{l} \text{sampling period:} \\ T_s = 0.1 \text{ s} \end{array} \right) \quad (36)$$

4.3.2 Control Law (35) Rewriting

In order to reduce transient guidance errors, vehicle control law (35) should anticipate steering action, in order to account for the delay introduced by the actuator. Of course, any situation faced by the vehicles cannot be anticipated: for instance ground irregularities, slippery parts of the field, etc., are completely unpredictable. Actually, the only reliable data on which anticipation can be achieved is the reference path curvature. For instance, in order to reduce guidance overshoots observed when the vehicles enter into a curve, control law values delivered to the actuator could be anticipated, in such a way that, when the vehicles actually enter into the curve, the actual steering angle is consistent with the curvature of the reference path, despite actuator delay. Lateral deviation could then stay close to zero during the transition phase.

In order to introduce such an anticipation into guidance law (35), this latter must first be split into two terms: the first one consisting in the contribution of the reference path curvature to the value of δ , and the second one gathering the contributions of deviations y

and $\tilde{\theta}$ and perturbation vector P . Model predictive control techniques will then be applied on the first term, but of course not on the second one.

To achieve such a separation, let us first consider the ideal case where the vehicle is perfectly on the path to be followed and sliding does not occur. In such a situation, the vehicle will stay on the reference path if the curvature defined by the vehicle steering angle is equal to the path curvature, i.e. steering angle δ must satisfy:

$$\frac{\tan \delta}{L} = c(s) \quad (37)$$

This geometric condition can be graphically checked on Figure 4. It can also be deduced from control law expression (35): if deviations $(y, \tilde{\theta})$ and sliding parameters $(\dot{Y}_P, \dot{\Theta}_P)$ are set equal to zero, the only term that is non-null inside the *arctan* parenthesis is the last one, and it provides relation (37) as expected.

Since the main contribution of the reference path curvature to the value of δ is provided by the last term in (35), this term is isolated below from the remaining terms in (35), in order to support anticipation in the forthcoming predictive guidance law. More precisely, let us define:

$$\mu = L \frac{c(s) \cos \tilde{\theta}}{1 - c(s)y} \quad (38)$$

$$\begin{aligned} \nu = L \left[\frac{\cos^3 \tilde{\theta}}{(1 - c(s)(y + y_c))^2} \left(\frac{dc(s)}{ds} (y + y_c) \tan \tilde{\theta} \right. \right. \\ \left. \left. - K_d(1 - c(s)(y + y_c)) \tan \tilde{\theta} - K_p(y + y_c) \right. \right. \\ \left. \left. + c(s)(1 - c(s)(y + y_c)) \tan^2 \tilde{\theta} \right) \right] \quad (39) \end{aligned}$$

Control law expression (35) can then be written as:

$$\delta = \arctan(\mu + \nu) \quad (40)$$

Relying now on trigonometric relation:

$$\arctan(a + b) = \arctan(a) + \arctan\left(\frac{b}{1 + a b + a^2}\right) \quad (41)$$

vehicle guidance law can finally be split as:

$$\delta = \delta_{Traj} + \delta_{Deviation} \quad (42)$$

$$\begin{aligned} \text{where:} \quad \delta_{Traj} &= \arctan(\mu) \\ \delta_{Deviation} &= \arctan\left(\frac{\nu}{1 + \mu \nu + \mu^2}\right) \end{aligned}$$

The two terms in the new guidance law expression (42) exhibit the expected features:

- δ_{Traj} is the main contribution of the reference path curvature to the value of δ . When deviations and sliding are equal to zero, δ_{Traj} provides with the expected value (37). This term will support forthcoming predictive control design.

- $\delta_{Deviation}$ is the contribution of deviations ($y, \tilde{\theta}$) and perturbation vector P (incorporated into y_c) to the value of δ . It aims at bringing y to 0. Since deviations and perturbations are unpredictable, $\delta_{Deviation}$ will remain unchanged in the forthcoming predictive control design.

4.3.3 Predictive Control Design

Model Predictive control techniques (see e.g. [14], [15]) can now be used to provide some anticipation in steering action, in order to reduce the transient guidance errors originating from actuator features. Beforehand, several conventions and notations have to be introduced:

- the k^{th} sample period is chosen below as the current time: state vector $X_{[k]}$ and perturbation vector $P_{[k]}$ are available, and the objective is to compute the steering angle value $\delta_{[k]}$ to be sent to the steering actuator.

- Prediction horizon H :

In predictive control approach, the current value of the control variables is computed from the current state and perturbation values, but also from the values that some variables should have in the future. H is the time (with respect to current time) when the values of these variables have to be predicted. H is a constant, and must be chosen with respect to the delay introduced by the actuator.

It is assumed below that $H = h T_s$, where T_s is the sample period, and h is an integer.

- Steering objective δ^{Obj} :

δ^{Obj} is the expected value for the actual steering angle δ_a at time $(k + h) T_s$, if at that time deviations and sliding effects were equal to 0.

More precisely, from the current values $s_{[k]}$ and $v_{[k]}$, the future $s_{[k+h]}$ value can be inferred, and δ^{Obj} can then be derived from relation (37).

- Steering measurement δ^{Meas} :

$\delta_{[k]}^{Meas}$ is the contribution of δ_{Traj} to the value of the actual steering angle δ_a at current time $k T_s$.

This variable, required in Model Predictive control approach, proposes here a difficulty, since definitely it cannot be measured: the complete control law $\delta = \delta_{Traj} + \delta_{Deviation}$ is always sent to the steering actuator. Therefore, the absolute encoder shown on Figure 13 cannot of course separate the contribution of the two terms in its single measurement $\delta_{a,[k]}$. In the sequel, $\delta_{[k]}^{Meas}$ has been approximated by:

$$\delta_{[k]}^{Meas} = \delta_{a,[k]} - \delta_{Deviation,[k]} \quad (43)$$

- Steering reference δ^{Ref} :

$(\delta_{[k]}^{Ref}, \delta_{[k+1]}^{Ref}, \dots, \delta_{[k+h]}^{Ref})$ is the desired trajectory, defined on the prediction horizon H , for the contribution of δ_{Traj} in the actual steering angle δ_a .

- the trajectory initial value $\delta_{[k]}^{Ref}$ is the actual contribution of δ_{Traj} in δ_a , such as provided by the encoder, i.e. $\delta_{[k]}^{Ref} = \delta_{[k]}^{Meas}$.
- the trajectory final value $\delta_{[k+h]}^{Ref}$ is the expected value at the end of the prediction horizon. Relying on the above notations, $\delta_{[k+h]}^{Ref} = \delta^{Obj}$.
- the trajectory linking these initial and final values has been derived according to a standard discrete first order relation:

$$\delta_{[k+i]}^{Ref} = \delta^{Obj} - \gamma^i \left(\delta^{Obj} - \delta_{[k]}^{Meas} \right) \quad i \in \{0, 1, \dots, h\} \quad (44)$$

where $\gamma \in]0, 1[$ is a free parameter that enables to shape the trajectory.

- Steering model output δ_a^{Model} :
 $(\delta_{a,[k]}^{Model}, \delta_{a,[k+1]}^{Model}, \dots, \delta_{a,[k+h]}^{Model})$ is the output of the steering actuator model (36) when the input is $(\delta_{Traj,[k-2]}, \dots, \delta_{Traj,[k+h-1]})$.
 - $\delta_{Traj,[k-2]}$ and $\delta_{Traj,[k-1]}$ are the actual δ_{Traj} values that have been used in control law (35) and sent previously to the actuator.
 - $(\delta_{Traj,[k]}, \dots, \delta_{Traj,[k+h-1]})$ are future δ_{Traj} values that are computed from the predictive algorithm detailed below.

These notations are also depicted on Figure 14.

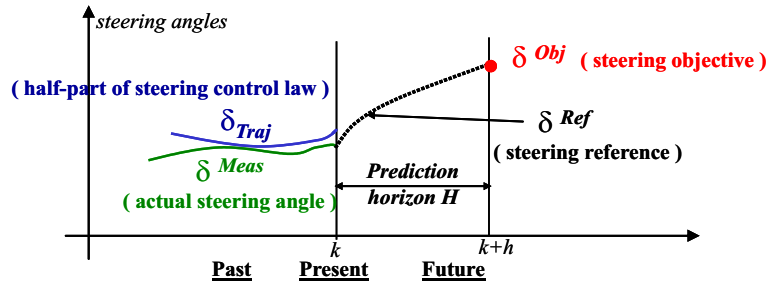


Figure 14: Notations used in Model Predictive Control design

Model Predictive Control design can now be sketched. Control law (35), previously designed in Section 4.2, provides at each sample period $k T_s$ with the steering angle value δ that is the most suitable to achieve path following. Unfortunately, this ideal control value is not instantaneously transmitted to the actual front wheels: it is sent to the steering actuation device that will transmit this ideal control value within some delay. Model Predictive Control proposes to anticipate the control value sent to the actuator, relying on the actuator model and on predictions on the future values to be taken by this control variable.

As above mentioned, the only reliable data on which prediction can be achieved is the reference path curvature. Therefore, control law (35) has been split into two terms, δ_{Traj}

and $\delta_{Deviation}$ (see expression (42)), and predictive control is now applied only on δ_{Traj} , which encloses the contribution of the reference path curvature to the value of δ . Model Predictive Control consists then in the following steps:

At each sample period kT_s :

- the value δ^{Obj} that the actual steering angle δ_a is expected to present in the forthcoming H seconds from the current time, is first computed relying on the reference path curvature.
- a trajectory δ^{Ref} which could lead the actual steering angle δ_a from its current value (corrected from $\delta_{Deviation}$, see (43)) to the desired one δ^{Obj} within H seconds is then computed. δ^{Ref} is given by (44).
- for any given future sequence of δ_{Traj} , the future sequence of the actual steering angle can be predicted, relying on actuator Model (36). The sequence $(\delta_{Traj,[k-2]}, \dots, \delta_{Traj,[k+h-1]})$ that can minimize the deviation between δ^{Model} and δ^{Ref} is then determined from optimization techniques. More precisely, the following problem is solved:

$$\begin{aligned} & \text{seek for } (\delta_{Traj,[k-2]}, \dots, \delta_{Traj,[k+h-1]}) \text{ such that} \\ & J = \sum_{i=0}^h (\delta_{[k+i]}^{Model} - \delta_{[k+i]}^{Ref})^2 \text{ is minimum} \end{aligned} \quad (45)$$

- The value of $\delta_{Traj,[k]}$ obtained from the optimal problem (45), named below $\delta_{Traj,[k]}^{Pred}$, is finally introduced into control law (42).

These computations are iteratively achieved at each further sample period. Therefore, vehicle guidance law accounting for actuator features can finally be written:

$$\delta = \delta_{Traj}^{Pred} + \delta_{Deviation} \quad (46)$$

The overall predictive control law is also depicted on Figure 15.

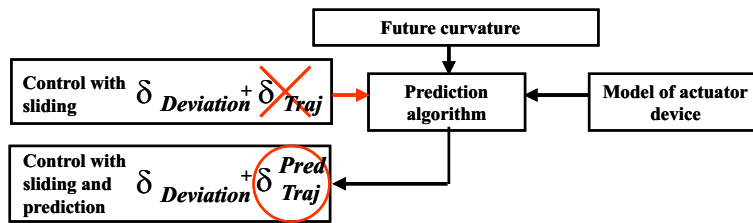


Figure 15: Model Predictive Control scheme

In order to account properly for actuator features, the optimization of criterion (45) should be performed on a duration superior or equal to the actuator rise time. For the steering device considered here, this imposes $H \geq 0.6$ s. However, in all experiments, a larger

value has been chosen for H , in order to account for steering actuator features, but also for unmodeled dynamic phenomena, such as the large vehicle inertia. These phenomena also introduce delays in the guidance feedback loop, and are therefore also responsible for the transient guidance errors. Enlarging the anticipation provided to δ_{Traj} can obviously reduce their effects. From experimental trials, $H = 1$ s has appeared as the most suitable value for the prediction horizon. Finally, γ has been set equal to 0.2 in order to provide δ^{Ref} with a smooth shape.

5 Experimental Results

In order to investigate the capabilities of the guidance laws designed in Section 4, numerous experiments have been carried out in our experimental farm at Montoldre, France.

The first experiments, reported in Section 5.1, have been performed on a level asphalted ground, in order that pure rolling and non-sliding conditions at wheels-ground contact points are satisfied. These experiments aim at highlighting the interesting features of non-linear control law (29), and therefore of control laws (35) and (46), since they are both designed from non-linear control law (29).

The other experiments, reported in Section 5.2, have been performed on agricultural fields. Curved path following on a slippery field, and straight line following on a sloping field are successively discussed. Abilities of control laws (35) and (46) to account respectively for sliding effects and for actuator features are demonstrated.

5.1 Guidance Laws Capabilities in the Absence of Sliding

In this section, it is shown that, as long as the vehicles do not undergo sliding effects, accurate curved path following can be achieved from non-linear control law (29). Additional attractive features of control law (29) are also highlighted.

5.1.1 Step Responses

Although step paths are not common in agriculture, such reference trajectories have first been considered as benchmarks, in order to investigate guidance accuracy when the vehicles describe straight lines and also the convergence features exhibited by control law (29).

Step responses at related velocities

The reference path consists in a 2 meters step. Experiments have been carried out at related velocities, from $v = 2$ km.h⁻¹ to $v = 14$ km.h⁻¹ with 2 km.h⁻¹ increments. Control law parameters have been tuned according to $(K_d, K_p) = (0.6, 0.09)$. This choice ensures that the error dynamics (28) presents a double pole located at the value 0.3. Linear control tools ensure then that a convergence without any overshoot and within a 15 meters settling distance is specified. This convergence rate has been chosen in order that the tractor motion, especially when its velocity is high, is not so steep that it would be uncomfortable to a

person in the tractor cabin. Moreover, it guarantees that actuators saturation is not met. The tractor trajectories are depicted on Figure 16.

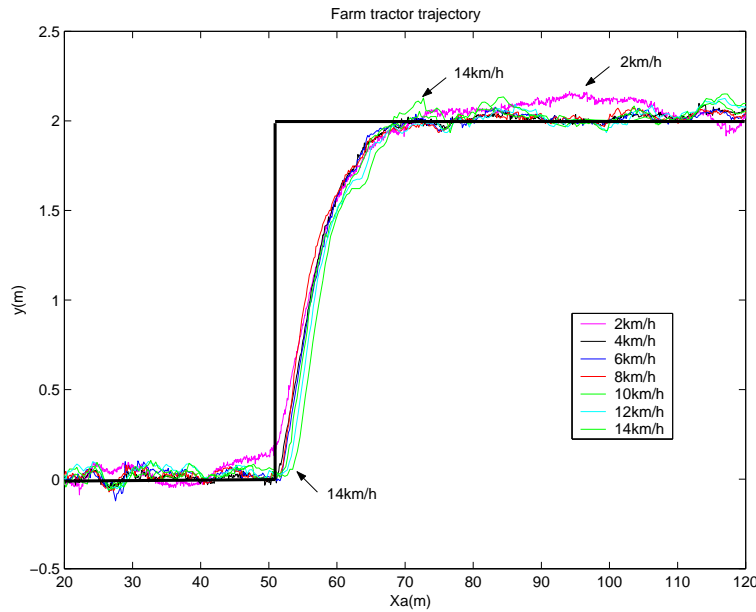


Figure 16: Tractor trajectories during step path following at related velocities

It can be seen on Figure 16 that all the step responses almost perfectly overlap: as expected, the trajectory is independent from the tractor velocity. Moreover, the 15 meters settling distance, specified when tuning the control parameters, is actually observed. This shows that, although control law (29) is a non-linear one, guidance performances tuning can be achieved in a very simple and intuitive fashion.

A thorough analysis establishes that, excepted for extreme velocities (i.e. $v = 2 \text{ km.h}^{-1}$ and $v = 14 \text{ km.h}^{-1}$), path following accuracy is quite satisfactory: once the tractor is following the second straight line (i.e. when $x_A > 70 \text{ m}$), the bias λ_y between the tractor trajectory and the reference path, as well as the tractor standard deviation from the mean trajectory σ_y , are both very small:

$$\text{in the worst case: } \lambda_y < 2.7 \text{ cm} \quad \sigma_y < 3.1 \text{ cm}$$

Finally, one can note that, when the step occurs, the tractor trajectories are more and more shifted when the speed is increased. Obviously, it is a consequence of the delay introduced by the steering actuator: the higher the tractor velocity is, the more the distance covered by the tractor before the steering angle actually changes its value is long.

When the tractor velocity reaches $v = 14 \text{ km.h}^{-1}$, the delay introduced by the actuator begins to damage path following performances. It can be observed from Figure 16: on one hand, the tractor starts to react few meters beyond step location, and on the other hand, the

tractor trajectory proposes a 10 centimeters overshoot when rejoining the new reference. $v = 14 \text{ km.h}^{-1}$ appears therefore as the maximum tractor velocity compatible with our steering device, when predictive control techniques are not investigated.

When the tractor velocity decreases to $v = 2 \text{ km.h}^{-1}$, the overall tractor trajectory is not satisfactory: it can be noticed from Figure 16 that the maximum deviation from the reference path, before or after step location, is beyond 10 centimeters. These very bad performances originate from the vehicle heading measurement. As detailed in Section 3.4, raw vehicle heading θ_t is computed, according to relation (13), from two successive vehicle position measurements provided by the RTK GPS sensor. Although this sensor provides position measurements with a very satisfactory 2 cm accuracy, the accuracy of vehicle heading θ_t is poor: 10.3° when $v = 8 \text{ km.h}^{-1}$, see Figure 8. Therefore a Kalman state reconstructor (15) has been designed in order to provide control laws with more reliable vehicle heading values. For vehicle velocities that are conventional in agricultural tasks (i.e. $v \approx 10 \text{ km.h}^{-1}$), the accuracy of reconstructed vehicle heading is satisfactory, see Table 2. However, the smaller the vehicle velocity is, the worse the accuracy of raw vehicle heading measurements θ_t is: for instance, at very low velocity $v = 2 \text{ km.h}^{-1}$, it can be computed from Figure 8 that the theoretical maximum heading measurement error climbs up to $\text{atan}(4/5.56)=35.7^\circ$. From such poor raw measurements, Kalman state reconstructor (15) cannot infer accurate vehicle heading values, so that the guidance law performances are necessarily damaged. This is one of the major difficulties that proceed from our initial choice to rely on a *single* RTK GPS receiver. However, it should be emphasized that $v = 2 \text{ km.h}^{-1}$ is a very low velocity, which is not typical in agricultural applications.

Step responses with a time-varying velocity

Experiments with a varying tractor velocity have also been carried out: the tractor velocity has been increased linearly from $v = 4 \text{ km.h}^{-1}$ to $v = 8 \text{ km.h}^{-1}$ when the tractor was performing the step response. Figure 17 displays the tractor trajectory thus obtained (graph *c*), superposed with two trajectories recorded with a constant tractor velocity (graph *a*: 4 km.h^{-1} , graph *b*: 8 km.h^{-1})

It can be observed on Figure 17 that all the trajectories are again superposed, and therefore that the 15 meters settling distance is achieved, even when the tractor velocity is varying. This establishes, as expected from the theoretical study presented in section 4.1, that control law (29) is actually velocity independent.

Step responses with large initial conditions

The last step response carried out is reported on Figure 18. It differs from the previous ones, since the initial conditions are very large: initially, the tractor is 10 meters far from the reference trajectory \mathcal{C} , and presents a very large heading error $\tilde{\theta} = 65^\circ$. The tractor velocity is $v = 6 \text{ km.h}^{-1}$.

Since control law (29) has been designed from the exact non-linear model of the tractor (no approximation, as for instance $\sin \tilde{\theta} \approx \tilde{\theta}$, has been performed), the error dynamics is

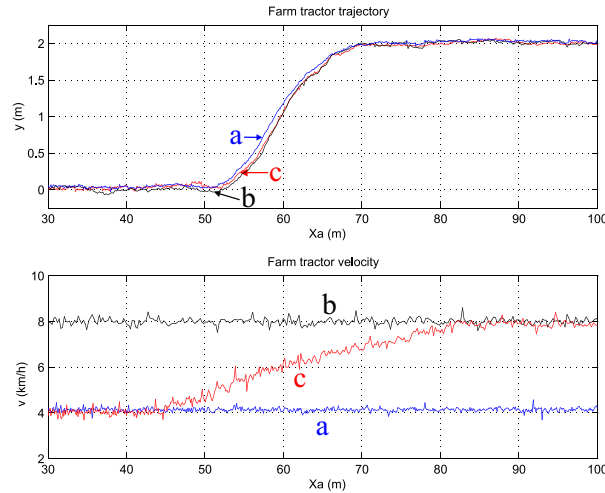


Figure 17: Tractor trajectories during step path following with constant velocities (graph *a*: $4 \text{ km}\cdot\text{h}^{-1}$, graph *b*: $8 \text{ km}\cdot\text{h}^{-1}$) or a time-varying velocity (graph *c*)

described *in an exact way* by the linear ODE (28), even if y and $\tilde{\theta}$ are very large. Therefore, it is expected that control law features remain identical to those reported previously.

Figure 18 shows that this theoretical result is actually achieved: it can be noticed from Figure 18(a) that the general appearance of the tractor trajectory is identical to that observed on Figure 16. Moreover, Figure 18(b) displays that heading deviation $\tilde{\theta}$ is exponentially decreasing within a settling distance equal to 15 meters, as expected.

5.1.2 Sine Curve Following

In order to investigate guidance law (29) capabilities when the reference trajectory is no longer a straight line but a curved path, sine curve following has been achieved. Sine curves are definitely not common trajectories in agricultural tasks. Nevertheless, they are significantly different from straight lines, and therefore can be seen as convincing benchmarks.

The curvature of the sinusoidal reference path has been chosen small (period and peak to peak amplitude are respectively 20 m and 60 cm) such that the vehicles do not undergo sliding when they are guided along this path. Therefore, the capabilities of guidance law (29) with respect to the reference path curvature can here be investigated independently from the incidence of sliding effects.

Experiments have been carried out with control and Kalman parameters K_d , K_p and L identical to those used in previous step response experiments (these parameters are henceforth never changed, even in Section 5.2). The tractor velocity is $v = 6 \text{ km}\cdot\text{h}^{-1}$, and the vehicle is initially 60 cm far from the reference trajectory. Its lateral deviation values are reported on Figure 19.

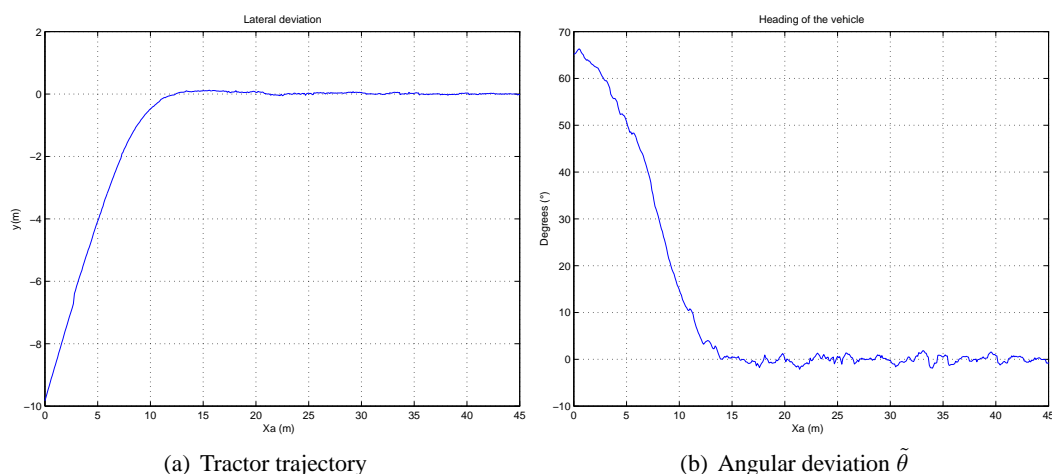


Figure 18: Convergence to a straight line from large initial conditions

It can be observed on Figure 19 that, as expected, control law (29) ensures the same guidance performances whatever the reference path features are: the settling distance and the statistical variables λ_y and σ_y recorded during this curved path following experiment are of the same order of magnitude than those previously recorded during step response experiments.

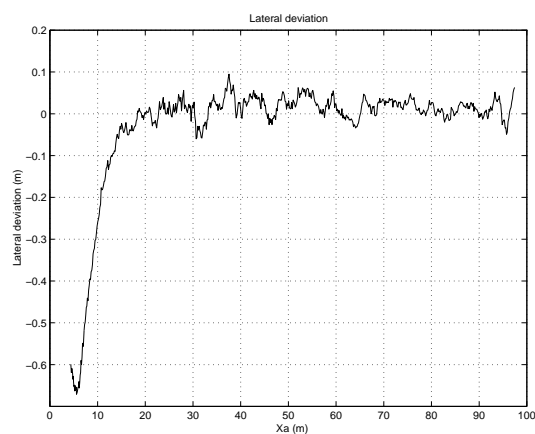


Figure 19: Lateral deviation with respect to a sinusoidal reference path

Due to numerous occurrences of $c(s)$, the expression of non-linear control law (29) is quite large. In order to investigate the actual contribution of the reference path curvature $c(s)$ in the satisfactory guidance performances displayed on Figure 19, sine curve following has also been experimented with the simplified control law (30) (a priori dedicated to straight line following) where $c(s)$ has been set equal to 0. Reference path, tractor trajec-

tory obtained with that law, and trajectory obtained with the entire control law (29), are displayed on Figure 20.

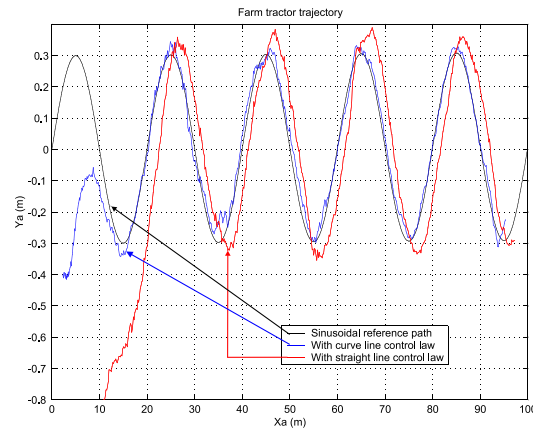


Figure 20: Tractor trajectories during a sine curve following: reference trajectory and trajectories obtained from control laws (29) and (30)

It can be observed that, without the reference path curvature information, the tractor follows the reference path with a 1.5 meters offset, and moreover presents large excursions when the values of $c(s)$ are the highest. This clearly establishes the relevancy of the reference path curvature information $c(s)$ used in non-linear guidance law (29).

5.2 Guidance Laws Capabilities with Respect to Sliding Effects

Experiments reported in this Section have no longer been performed on asphalt but, as it is expected in agricultural tasks, on land fields.

When the vehicles move on a level compact ground, guidance results are absolutely similar to those presented in Section 5.1, whatever the guidance law is: since adaptive control law (35) and predictive law (46) have both been designed from non-linear control law (29), the performances and the attractive features of the latter one are propagated to the two former ones.

Therefore, experiments reported in this Section address specifically situations where sliding occurs. Vehicle behavior, and especially a loss in accuracy when automatic guidance relies on non-linear control law (29), is displayed. The relevancy of the approaches proposed to account for sliding effects in vehicle modeling and control (Model (11) and adaptive control law (35)), and to account for the actuator features (predictive control law (46)), are then demonstrated.

More precisely, three reference trajectories have been successively considered. The first one consists in a long curve to be achieved on a level slippery ground. Sliding effects occur when the vehicle enters into the curve, and since the reference path curvature is almost constant, the capabilities of the proposed control approaches with respect to quite constant

sliding conditions can be investigated. The second reference path consists in a succession of half-turns on the same level slippery ground. Guidance accuracy, when sliding conditions are continuously varying, can then be addressed. The last reference path consists in a straight line to be achieved on a sloping field. Control laws capabilities, when sliding effects originate no longer from path curvature but from slope, can then be investigated. Additional experimental results can also be found in [8] and [9].

5.2.1 Guidance on Level Slippery Fields when the Path Curvature is Constant

Automatic guidance has first been achieved with respect to the reference path shown on Figure 21. This path, named below path #1, has not been computed from a GPS map of the field: the farm tractor has been manually driven, and the path has then been recorded from the position measurements provided by the RTK GPS sensor on-boarded. This is a simple and convenient method to be sure that the farm tractor can actually follow the assigned reference path.

This reference path consists mainly in a long curve (three quarters of a circle) achieved on a level slippery ground. Poor adherence conditions at wheels-ground contact points, reference path large curvature ($c(s) \approx 0.2 \text{ m}^{-1}$), and vehicle large inertia explain that sliding occurs when the farm tractor is describing the curved part of the path.

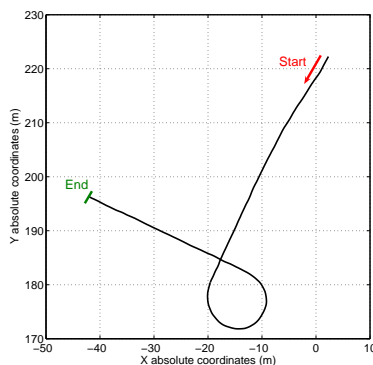


Figure 21: Reference path # 1

Experimental validation of Model (11) and sliding estimation (16)

The capability of the vehicle extended kinematic Model (11) designed in Section 3.3 to account properly for sliding effects is first investigated via the experiments reported on Figure 22.

More precisely, path #1 following has been achieved at a constant velocity $v = 8 \text{ km.h}^{-1}$, relying on non-linear control law (29). Since the curvature is quite constant in the curved part of path #1, sliding effects are also expected to be constant. In that case, extended kinematic Model (11) predicts that lateral and angular deviations converge to some

constant (see Section 4.2), whose values could be computed from (31) and (34) if \dot{Y}_P and $\dot{\Theta}_P$ values were known.

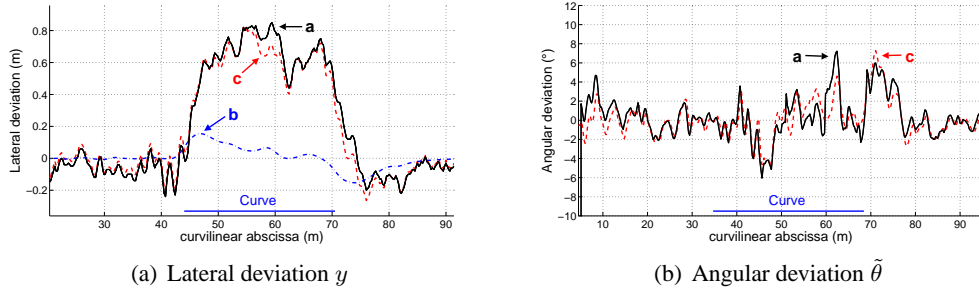


Figure 22: Deviations during path #1 following with control law (29): actual deviation (solid - a) and simulated ones from Models (10) (dash-dotted - b) and (11) (dashed - c)

Lateral and angular deviations recorded during this experiment are depicted in solid line on Figures 22. The lateral deviation shown on Figure 22(a) fits exactly with the behavior predicted by Model (11): when the vehicle is describing the first straight line part of path #1 ($s < 45$ m), its lateral deviation is close to zero, as it is expected from control law (29) since no sliding occurs. In contrast, when the vehicle enters into the curve ($s = 45$ m), it undergoes sliding effects. It can be observed that a lateral deviation then appears, and remains quite constant ($y \approx 70$ cm) as long as the vehicle is describing the curve. Finally, this lateral deviation returns to zero when the vehicle exits from the curve ($s > 72$ m). The asymptotic value of the lateral deviation during the curved part of path #1 cannot however be verified, since we have no access to \dot{Y}_P and $\dot{\Theta}_P$ values.

Figure 22(b) displays the angular deviation recorded during the same experiment. Observations are more difficult since the noise ratio on that measurement is more important than on lateral deviation measurement. This is always a consequence of the difficulty to have access to vehicle heading θ_t when relying solely on an RTK GPS sensor, as it has been extensively discussed above. Nevertheless, it can be noticed that during the straight line parts of path #1, the mean value of the angular deviation is zero, as it is expected from control law (29) since no sliding occurs. In contrast, when the vehicle is describing the curved part of path #1, the angular deviation then exhibits a non-null mean value, slightly inferior to 2° . This also agrees with what could be predicted from Model (11), see relation (31). The non-null mean value of angular deviation $\tilde{\theta}$ reveals that the vehicle is slightly moving crabwise.

The experiment reported on Figure 22 demonstrates that vehicle extended kinematic Model (11) can properly account for sliding effects, at least when these latter are constant. In order now to investigate if sliding estimation algorithm (16) can provide with satisfactory information, two simulations have been run:

- the first one, depicted in dash-dotted line on Figure 22, is path #1 following simulation, relying on Model (10), i.e. vehicle model without sliding accounted.

- the second one, depicted in dashed line on Figure 22, is also path #1 following simulation, but relying this time on Model (11). The perturbation information \dot{Y}_P and $\dot{\Theta}_P$ introduced in that simulation have been provided by sliding estimation algorithm (16) that had been run during the above mentioned experiment, i.e. during path #1 following carried out with the farm tractor.

It can be observed on Figure 22(a) that the lateral deviation simulated from Model (11) fits almost perfectly with the actual lateral deviation recorded during the experiment:

- first, this simulation provides with the same 70 cm lateral deviation when the vehicle is describing the curved part of path #1,
- moreover, even the small variations of the actual lateral deviation (variations centered on 0 during straight line following, and centered on 70 cm when the farm tractor is describing the curve) are also reproduced on the simulation.

The angular deviation simulated from Model (11), shown on Figure 22(b), presents also satisfactory results:

- during straight line following, the simulated angular deviation also fits perfectly with the actual one: once more, even the small variations of the actual angular deviation are reproduced on the simulation.
- in contrast, when the vehicle is describing the curved part of path #1, the two curves are no longer overlapping. These differences originate from the method followed to measure the vehicle heading: raw vehicle heading measurement (13), as well as Kalman reconstructor equations (15), rely on pure rolling and non-sliding conditions at wheels-ground contact points. However, these conditions are no longer satisfied when the vehicle is describing the curved part of path #1. Therefore, in that situation, the vehicle heading reconstruction θ_t is not very accurate, which leads to the small inconsistencies noticed on Figure 22(b). Nevertheless, the simulated angular deviation presents the expected main feature, i.e. a non-null mean value.

In contrast, the simulation run from Model (10) provides with deviations that may be far from the actual ones. It can be observed on Figure 22(a) that:

- the lateral deviation simulated from Model (10) is exactly zero during straight line following. This is quite normal, since it is a purely theoretical simulation: no actual information is ever accounted in Model (10).
- this simulated lateral deviation presents only some overshoots when the vehicle is describing the curved part of path #1: these overshoots are generated by the delay introduced by the steering actuator (since actuator features are accounted in both simulations). They occur each time path #1 curvature presents fast variations (especially at the beginning/end of the curved part of path #1).

Since the lateral deviation simulated from Model (10) is close to zero even during the curved part of path #1, control law (29) (which has been designed from Model (10)) cannot be aware that special steering corrections are demanded in that case. This explains that in actual experiments, that control law leads to a non-satisfactory permanent lateral deviation. In contrast, the second simulation has revealed that vehicle extended kinematic Model (11), together with sliding estimation algorithm (16), can describe very accurately the vehicle behavior in presence of sliding. Therefore, this model and this estimation algorithm appear actually reliable to support control design refinements which could account for sliding effects, and then ensure a null lateral deviation in the curved part of path #1. These control designs have been presented in Sections 4.2 and 4.3. Capabilities of the proposed guidance laws (35) and (46) are now investigated, still with respect to path #1 following experiments.

Guidance capabilities of adaptive control law (35)

First, path #1 following has been achieved, at constant velocity $v = 8 \text{ km.h}^{-1}$, relying on adaptive control law (35). The two approaches proposed in Section 4.2 in order to compute the adaptive corrective term y_c , i.e. MRAC and IMC schemes, have both been experimented. Guidance capabilities are displayed on Figure 23, and compared with those previously obtained with non-linear control law (29). More precisely, the conventions used on Figure 23 are:

- solid line: path following achieved from non-linear control law (29),
- dash-dotted line: path following achieved from adaptive control law (35), when the corrective term y_c is computed from MRAC scheme,
- dashed line: path following achieved from adaptive control law (35), when the corrective term y_c is computed from IMC scheme.

It can be observed on Figure 23(a) that, as expected, both adaptive control laws succeed in bringing back the vehicle lateral deviation close to zero during the curved part of path #1, despite sliding occurrence: when non-linear guidance law (29) leaves the vehicle 70 cm far from its reference trajectory during the whole curved part of the path, both adaptive laws (35) provide a more satisfactory 15 cm guidance accuracy during the main part of the same curve. More precisely, adaptive guidance law relying on IMC scheme ensures that, when $s \in [50 \text{ m}, 65 \text{ m}]$, the vehicle lateral deviation displays a satisfactory 6 cm mean value and a 6 cm standard deviation from the mean.

Nevertheless, it has also to be noticed on Figure 23(a) that adaptive control laws (35) cannot prevent from large transient guidance errors at the beginning/end of the curved part of path #1. At those places, path #1 curvature, and therefore sliding conditions, present fast variations. Due to the delay introduced mainly by the actuator device, the vehicle steering angle cannot react immediately, so that the vehicle transiently deviates from path #1. This very disappointing behavior has been addressed in Section 4.3, relying on Model Predictive

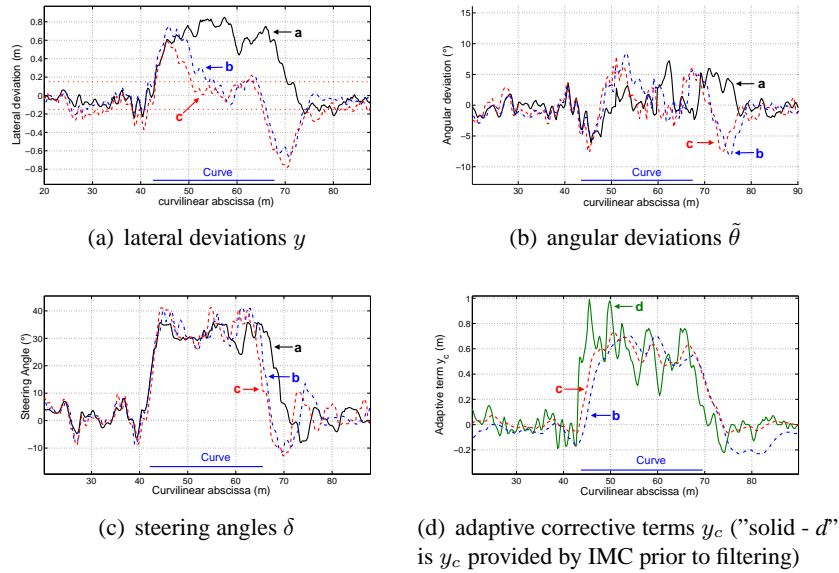


Figure 23: Capabilities of non-linear control law (29) (solid - a), adaptive control laws (35) relying on MRAC scheme (dash-dotted - b) and IMC scheme (dashed - c)

control techniques. Capabilities of the proposed control law (46) with respect to these transient guidance errors are investigated in forthcoming experiments reports (see Figure 24).

It can also be observed on Figure 23 that the two adaptive schemes, i.e. MRAC and IMC, present very similar performances. From a theoretical point of view, it was expected that IMC scheme could enable to fit more accurately with the current sliding conditions, and therefore could provide with more accurate guidance capabilities: with IMC scheme, the adaptive corrective term y_c is always the most suitable one for any given perturbation values \dot{Y}_P and $\dot{\Theta}_P$, since it is computed directly from the asymptotic relation (34). In contrast, with the MRAC scheme, perturbation values \dot{Y}_P and $\dot{\Theta}_P$ are proceeded through a simulation application, which obviously acts as a low-pass filter when delivering y_c value.

This expected behavior for y_c values is actually obtained: Figure 23(d) displays y_c values provided by MRAC scheme in dash-dotted line as usual, and those directly provided by IMC scheme in solid line. It can be observed that, as soon as the vehicle enters into the curve, the y_c values supplied by IMC scheme are instantaneously close to the constant value that they should have during the whole curve (since path #1 curvature, and therefore sliding conditions, are constant). However, this positive feature is counterbalanced by a very negative one: the y_c values supplied by IMC scheme present a very poor noise ratio, and would obviously lead to oscillations on steering angle δ , if they were sent directly to adaptive control law (35). As it has been mentioned in Section 3.4.1, numerous perturbations, and not only sliding effects, are accounted in \dot{Y}_P and $\dot{\Theta}_P$ values provided by estimation algorithm (16). Therefore, \dot{Y}_P and $\dot{\Theta}_P$ present a poor noise ratio, and the same feature is

propagated to y_c via relation (34). Consequently, as it has been announced in Section 4.2, the y_c values supplied directly from IMC scheme have to be filtered. The values actually used in adaptive control law (35) are shown in dashed line on Figure 23(d), and are then no longer very different from those provided by MRAC scheme. Therefore, guidance capabilities offered by the two schemes are quite similar, as it can be observed on Figure 23(a).

Finally, the vehicle behavior during curved part of path #1 can be further analyzed from Figures 23(b) and 23(c). When the vehicle is guided according to non-linear control law (29), its angular deviation does not present noticeable changes when the curve is described: it can just be noticed on Figure 23(b) that the angular deviation mean value becomes slightly non-null ($\approx 2^\circ$) during the curve, indicating that the vehicle presents a slight crabwise motion. In contrast, when the vehicle is guided according to adaptive control law (35), its angular deviation presents higher values ($\approx 8^\circ$) at the beginning of the curve, indicating that the vehicle is turning to join back reference path #1. This is also corroborated by higher steering angle values, as shown on Figure 23(c): adaptive control law (35) is clearly acting in order to reject sliding effects. Similar behavior can be observed when the vehicle is exiting from the curve. When it is guided according to non-linear control law (29), the vehicle is 70 cm aside from path #1 when the curve is described. When it reaches the end of this curve, no noticeable change is observed on its angular deviation $\tilde{\theta}$: the vehicle joins back path #1 just because sliding effects have disappeared. In contrast, when the vehicle is guided according to adaptive control law (35), it is close to path #1 when the curve is described. When it reaches the end of this curve, sliding effects suddenly vanish. Due to the delay introduced by the steering actuator, the vehicle transiently diverges from path #1, leading to a negative angular deviation, as it can be noticed on Figure 23(b), and negative steering angle values in order to bring back the vehicle on path #1, as it can be observed on Figure 23(c).

Guidance capabilities of predictive control law (46)

Finally, path #1 following has also been achieved, still at constant velocity $v = 8 \text{ km.h}^{-1}$, relying this time on predictive control law (46). The two possibilities for computing the adaptive corrective term y_c , i.e. MRAC and IMC schemes, have still been experimented. Guidance capabilities are reported on Figure 24, and are always compared with those previously obtained with non-linear control law (29). The convention used on Figure 24 are similar to the conventions previously introduced on Figure 23:

- solid line: path following achieved from non-linear control law (29),
- dash-dotted line: path following achieved from predictive control law (46), when the corrective term y_c is computed from MRAC scheme,
- dashed line: path following achieved from predictive control law (46), when the corrective term y_c is computed from IMC scheme.

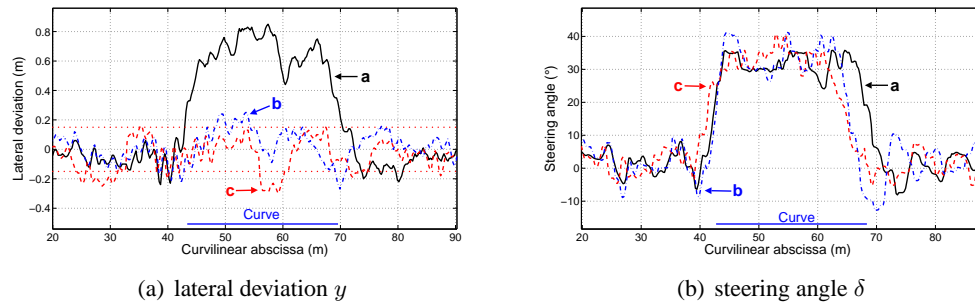


Figure 24: Capabilities of non-linear control law (29) (solid - a), predictive control laws (46) relying on MRAC scheme (dash-dotted - b) and IMC scheme (dashed - c)

Figure 24 demonstrates that, when the vehicles are guided according to predictive control laws (46), path #1 following can then be achieved without any large transient guidance error at the beginning/end of the curve. As detailed in Section 4.3, prediction only relies on reference path curvature information: the steering action is anticipated (with respect to the delay introduced by the actuator) when path #1 curvature is about to change, i.e. at the beginning/end of the curved part. Therefore, when the vehicle actually enters into the curve, or exits from the curve, actual steering angle δ_a displays a value consistent with path #1 current curvature. The adaptive corrective parameter y_c , still present in predictive control law (46), can then efficiently account for sliding effects as soon as they appear/disappear, so that an accurate path following can be achieved for the path long. Figure 24(a) shows that the vehicle lateral deviation belongs to the acceptance range of ± 15 cm for most of the path #1 following experiment. The disturbance observed when $s \in [55$ cm, 60 cm] is due to a hole on the ground crossed by the tractor, which is of course an unpredictable event.

Capabilities of the proposed guidance laws when the vehicles undergo sliding effects are summarized in Table 3. For all the guidance laws (excepted of course for non-linear control law (29)), these statistical computations have been carried out when the adaptive corrective term y_c is provided by IMC scheme (similar performances are however also obtained with MRAC scheme, see Figure 24(a)). More precisely:

- for non-linear control law (29) and predictive control law (46), the mean lateral deviation value and its standard deviation from the mean have both been computed when the vehicle is describing the curved part of path #1, i.e. when $s \in [45$ cm, 65 cm].
- for adaptive control law (35), these two quantities have been computed only when the vehicle has joined back path #1 in the curved part of this path, i.e. when $s \in [52$ cm, 65 cm]. By this way, the statistical quantities are not polluted by actuator features and reflect actually guidance law capabilities with respect to sliding effects.
- the two other quantities in Table 3 provide with the range of variation of the vehicle lateral deviation. In the case of adaptive control law (35), they indicate the amplitude of the transient guidance errors due to steering actuator features.

Table 3: Statistical data on vehicle lateral deviation on the curved part of path #1

	mean value	std value	min value	max value
non-linear control law (29)	70 <i>cm</i>	9 <i>cm</i>	44 <i>cm</i>	85 <i>cm</i>
adaptive control law (35)	6 <i>cm</i> (overshoots excepted)	6 <i>cm</i>	-78 <i>cm</i>	59 <i>cm</i>
predictive control law (46)	-3 <i>cm</i>	12 <i>cm</i>	-30 <i>cm</i>	15 <i>cm</i>

Finally, Figure 24(b) reports steering angle values during path #1 following. The anticipation in the steering action, introduced by predictive control law (46), appears clearly when considering the experimental data recorded when the adaptive corrective term y_c is provided according to IMC scheme: steering angle δ is actually increasing prior to the beginning of the curve. Steering values are, as expected, anticipated with respect to the ones recorded when the vehicle is guided according to non-linear control law (29). The same steering behavior is observed at the end of the curve.

When the adaptive corrective term y_c is provided according to MRAC scheme, anticipation is not obvious at the beginning of the curve, just because the steering angle was accidentally negative ($\approx -10^\circ$) at the instant when the anticipation should have started. Moreover, since MRAC scheme accounts for sliding in a slightly slower fashion than IMC scheme, the steering angle must finally climb to higher values than with IMC scheme (41° vs 35°) in order to keep the vehicle on path #1. At the end of the curve, the anticipation provided by MRAC scheme can be observed, but higher negative steering values than with IMC scheme are however noticed, due once more to the way sliding is accounted.

5.2.2 Guidance on Level Slippery Fields when the Path Curvature is Varying

Path #1 following experiments have demonstrated that predictive control law (46) can ensure an accurate guidance when the vehicles undergo a constant sliding (sliding effects are expected to be constant, since the curved part of path #1 presents a constant curvature). In order to investigate guidance law (46) capabilities with respect to reference trajectories where sliding effects are no longer constant, automatic guidance has been achieved with respect to the path depicted on Figure 25, named below path #2.

This path has also been recorded from the position measurements provided by the RTK GPS sensor on-boarded, when the farm tractor has been once manually driven. Experiments have been carried out on the same slippery ground than for path #1. Therefore, the same sliding effects than those observed during path #1 following are qualitatively expected when the farm tractor is describing the curved parts of path #2. However, since path #2 presents both positive and negative curvatures, sliding effects change their direction during the completion of this path. Moreover, since the straight lines linking the half-turns are very short, the variations from positive sliding effects to negative ones are very fast. It is a very unfavorable situation that actually allows to investigate guidance laws capabilities when sliding conditions are varying.

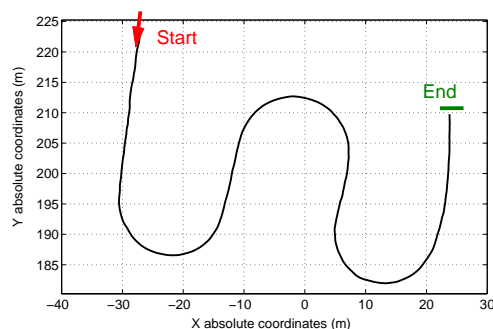


Figure 25: Reference path # 2

Path #2 following has also been achieved at a constant velocity $v = 8 \text{ km.h}^{-1}$. Adaptive control law (35) and predictive control law (46) have both been experimented. In both cases, the adaptive corrective term y_c has been supplied from IMC scheme. Non-linear control law (29) has also been experimented, in order to provide with a comparison. Vehicle lateral deviations are reported on Figure 26, with the following conventions:

- solid line: path following achieved from non-linear control law (29),
- dash-dotted line: path following achieved from adaptive control law (35), when the corrective term y_c is computed from IMC scheme,
- dashed line: path following achieved from predictive control law (46), when the corrective term y_c is computed from IMC scheme.

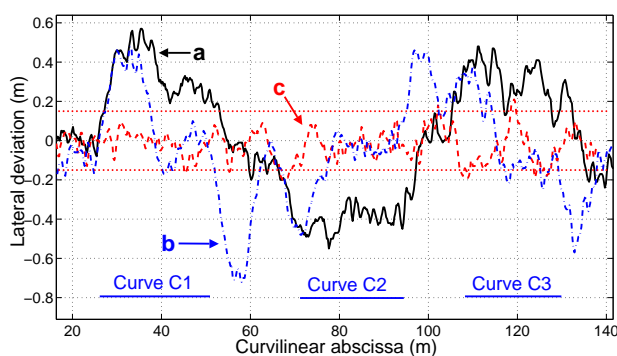


Figure 26: Lateral deviations recorded during path #2 following achieved from non-linear law (29) (solid - a), adaptive law (35) (dash-dotted - b), predictive law (46) (dashed - c)

First, it can be observed on Figure 26 that the vehicles guided according to non-linear control law (29) present large lateral deviations in each curved part of path #2, due obviously to sliding occurrences. The lateral deviation is successively positive and negative,

depending on sliding effects direction. In contrast, guidance accuracy obtained with predictive control law (46) belongs satisfactorily to the acceptance range of ± 15 cm during the whole path #2. Although the adaptive corrective term y_c used to account for sliding effects has been designed relying on a constant sliding assumption (see Section 4.2), the online update of this parameter allows nevertheless to address satisfactorily situations where sliding effects are varying. Therefore, this proposed guidance law can actually deal with this very unfavorable situation, rarely encountered in agricultural tasks.

Figure 26 points also out the importance of the predictive part in control law (46). When this control refinement is not used, i.e. when automatic guidance is achieved according to adaptive control law (35), guidance accuracy is actually very poor: when the vehicle enters into the first curve, a large transient guidance error occurs, as it is expected since the steering actuator introduces a delay. Then, adaptive control law (35) accounts for sliding effects and brings the vehicle back on path #2. However, this path is constituted from a succession of short curves. Therefore, when the vehicle joins back the reference path, the first curve is already ended, and a second guidance overshoot occurs, and so on with the two other curved parts of path #2. Finally, due to the numerous overshoots, the guidance accuracy is almost as poor as when non-linear control law (29) is used. This demonstrates that, in order to follow with a satisfactory accuracy a path whose curvature is varying, it is mandatory to account for actuator features. Model Predictive Control techniques, used to design control law (46), have been shown to be a very efficient approach to address this problem.

5.2.3 Straight Line Following on a Sloping Field

In the above experiments, the farm tractor undergoes sliding effects since it is describing paths with large curvatures on a level slippery ground. Experiments reports have revealed that vehicle extended kinematic Model (11) and sliding estimation algorithm (16) can properly account for such sliding effects, and that the proposed control laws can provide with a satisfactory guidance accuracy, despite sliding occurrence.

However, vehicles can also undergo sliding effects when describing straight lines on a sloping field. The experiments reported below aim at demonstrating that the proposed modeling, sliding estimation and guidance law design are also relevant to address sliding effects originating from slope.

The last automatic guidance experiments have therefore been achieved with respect to the path shown on Figure 27, and named below path #3. This path is almost a straight line, achieved on a sloping field, perpendicularly to the slope (indicated by the arrows on Figure 27). All along this path, the field slope is slightly varying around a mean value equal to 15%. Poor adherence conditions at wheels-ground contact points, and gravity forces originating from vehicle large inertia and field slope, explain that sliding occurs permanently when the farm tractor is describing this path.

Experimental validation of Model (11) and sliding estimation (16)

In order to investigate the ability of vehicle extended kinematic Model (11) to account

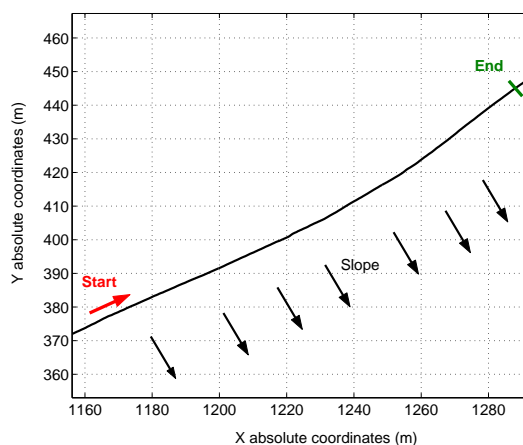


Figure 27: Reference path #3

properly for sliding effects originating from slope, path #3 following has been achieved at a constant velocity $v = 6 \text{ km.h}^{-1}$, relying on non-linear control law (29). Since the slope is quite constant all along this reference path, sliding effects are also expected to be constant. Therefore, it is finally the same situation than the one obtained when the vehicles are describing a path with a constant curvature on a level slippery ground, although sliding effects are not originating exactly from the same physical phenomena. As it has been mentioned above, extended kinematic Model (11) predicts in that case that the vehicle lateral and angular deviations converge to some constants (see Section 4.2), whose values could be computed from (31) and (34) if \dot{Y}_P and $\dot{\Theta}_P$ values were known.

The deviations recorded during this experiment are depicted in solid line on Figures 28. The vehicle lateral deviation shown on Figure 28(a) does not present a constant non-null value, as it was expected: it can be observed that the vehicle is oscillating within a very large 80 cm strip aside from path #3. It is however immediate to note that this strip is definitely not centered on the reference path. Therefore, if only the mean value of the lateral deviation is regarded, a large non-null value is then obtained (close to 30 cm), which is somehow consistent with what was expected from Model (11).

The large oscillations displayed by the vehicle can be explained by:

- the field slope, which is probably not perfectly constant along path #3,
- the tractor cabin oscillations: when a vehicle is moving perpendicularly to a slope, the mass distribution on the vehicle is noticeably modified. Therefore, the two shock absorbers located on the opposite side from the slope are more compressed than the two others, thus leading to tractor cabin oscillations. Since the GPS antenna is located on the top of the cabin, position measurements provided by the RTK GPS sensor are likely to present also some oscillations, which are directly reflected on lateral deviation measurements shown on Figure 28(a).

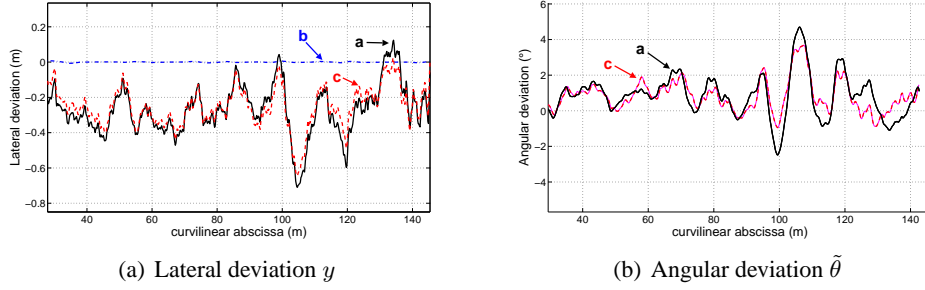


Figure 28: Deviations during path #3 following with control law (29): actual deviation (solid - a) and simulated ones from Models (10) (dash-dotted - b) and (11) (dashed - c)

The vehicle angular deviation recorded during the same experiment is displayed on Figure 28(b). It has been abundantly mentioned above that vehicle heading measurement is a critical point in our application, even in the most favorable situation, since it relies on a single RTK-GPS sensor. With respect to vehicle heading measurement, the current experiment is undoubtedly far from the most favorable situation: the tractor cabin presents oscillations, pure rolling and non-sliding conditions at wheels-ground contact points (which are explicitly used to derive θ_t) are not satisfied, and moreover sliding effects are varying since the field slope is probably not constant. Therefore, it is not surprising to observe a very oscillating angular deviation $\tilde{\theta}$ on Figure 28(b). However, if once more only the mean value of the deviation is regarded, a non-null value is clearly obtained ($\approx 1^\circ$), which is again consistent with what could be predicted from Model (11), see relation (31). This non-null mean value for the angular deviation $\tilde{\theta}$ reveals that, as in path #1 following, the vehicle is slightly moving crabwise.

Vehicle extended kinematic Model (11) appears therefore consistent with the experimental results reported on Figure 28, at least if only mean deviation values are regarded. In order now to investigate if sliding estimation algorithm (16) can provide with satisfactory information, two simulations have again been run. They are exactly similar to those achieved when investigating sliding estimation algorithm (16) with respect to path #1. The conventions used on Figure 28 are also similar:

- path #3 following simulation relying on Model (10) (i.e. vehicle model without sliding accounted) is shown in dash-dotted line.
- path #3 following simulation relying on Model (11) is shown in dashed line. The perturbation information \dot{Y}_P and $\dot{\Theta}_P$ introduced in that simulation are provided by sliding estimation algorithm (16) that had been run during the above mentioned experiment, i.e. when the farm tractor was achieving path #3 following.

As it was expected, Model (10) cannot describe the actual vehicle behavior: since no actual information is accounted in Model (10), this simulation is a purely theoretical one, providing with a constantly null simulated lateral deviation, when the actual lateral deviation is non-null and varying, see Figure 28(a).

In contrast, it can be observed on Figure 28(a) that the lateral deviation simulated from Model (11) fits perfectly with the actual lateral deviation recorded during the experiment: even the small variations of the actual lateral deviation are reproduced on the simulation. Simulated and actual angular deviations are also satisfactorily consistent, as it is displayed on Figure 28(b). Small differences can be noticed, but they are inherent to the vehicle heading measurement method, which is not completely correct when the vehicles undergo sliding effects (this point has already been discussed when sliding estimation algorithm (16) had been investigated with respect to path #1). Therefore, extended kinematic Model (11), together with sliding estimation algorithm (16), appear actually reliable to describe the vehicle behavior, not only when sliding effects originate from reference path curvature, but also when they originate from slope.

Adaptive and predictive guidance laws (35)-(46), designed from Model (11), have been shown, in the above reported experiments, to be efficient when sliding effects originate from reference path curvature. It is shown below that they can also provide with satisfactory guidance results when sliding effects originate from slope.

Guidance capabilities of adaptive control laws (35)

Path #3 following has therefore been achieved, at constant velocity $v = 6 \text{ km.h}^{-1}$. Predictive control laws (46), designed in Section 4.3, aim at providing anticipation to the steering action from reference path curvature information. However, since path #3 consists in a straight line, no anticipation can actually be provided, so that predictive control laws (46) are exactly identical to adaptive control laws (35) in this application. Therefore, only experimental results obtained with these latter guidance laws are shown on Figure 29. Once more, the two approaches proposed in Section 4.2 in order to compute the adaptive corrective term y_c , i.e. MRAC and IMC schemes, have both been experimented. Guidance capabilities obtained with non-linear control law (29) are also reported in order to provide with a comparison. The conventions used on Figure 29 are similar to the conventions previously used on Figure 23 to display path #1 following reports:

- solid line: path following achieved from non-linear control law (29),
- dash-dotted line: path following achieved from adaptive control law (35), when the corrective term y_c is computed from MRAC scheme,
- dashed line: path following achieved from adaptive control law (35), when the corrective term y_c is computed from IMC scheme.

It can be observed on Figure 29(a) that, whatever the guidance law is, the farm tractor describes the reference straight line with noticeable oscillations. The measurement device on-boarded on the tractor has a large responsibility in this oscillating behavior: in such an unfavorable situation, this device relying solely on an RTK-GPS sensor, is not able to provide with accurate enough state measurements:

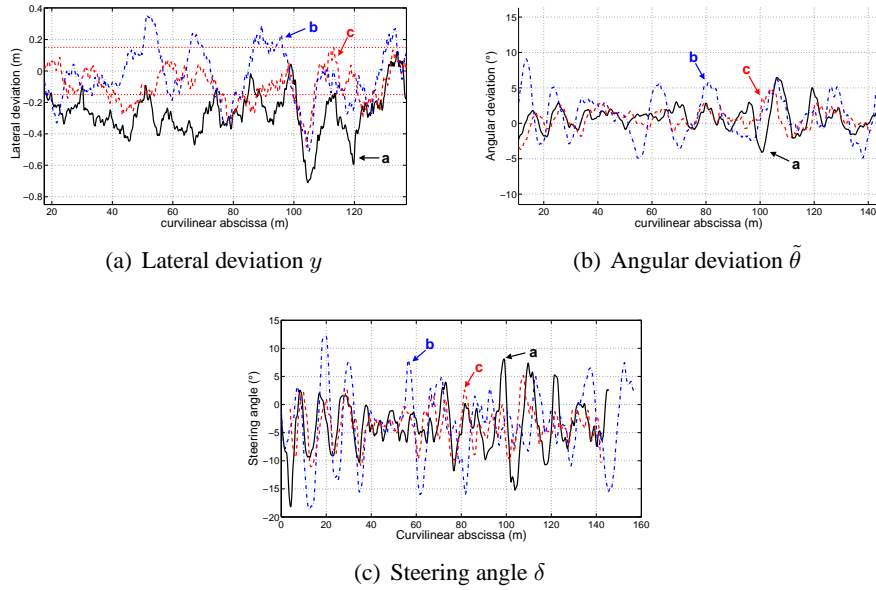


Figure 29: Capabilities of non-linear control law (29) (solid - a), adaptive control laws (35) relying on MRAC scheme (dash-dotted - b) and IMC scheme (dashed - c)

- the GPS antenna is located on the top of the tractor cabin. Therefore, due to the above mentioned tractor cabin oscillations, the position measurements supplied by the RTK-GPS sensor are obviously not as reliable as they were in guidance applications achieved on a level ground.
- raw vehicle heading measurements θ_t are, according to (13), computed from two successive position measurements. Therefore, the slight inaccuracy in these latter measurements is also propagated to raw θ_t measurements.
- finally, both raw vehicle heading measurements (13) and Kalman reconstructor equations (15) have been derived according to pure rolling and non-sliding conditions at wheels-ground contact points. However, when a vehicle is moving on a sloping field, these conditions are constantly unsatisfied. This is corroborated by Figure 29(b): the vehicle angular deviation is continuously presenting a non-null value, indicating that the vehicle is continuously moving crabwise (this occurs only from time to time when the vehicle was describing a curve on a level ground).

This less reliability of position and heading measurements can explain for a large part the oscillating feature exhibited by the vehicle lateral deviation on Figure 29(a). Nevertheless, it is worth noticing that both adaptive control laws (35) provide, when compared with non-linear control law (29), with a significantly more accurate vehicle guidance. To quantify this point, the time spent by the farm tractor within a ± 15 cm strip centered on the reference path has been computed for each guidance law. These data have then been converted into

a percentage and reported in Table 4, which displays clearly the improvement in guidance accuracy.

Table 4: Guidance accuracy during path #3 following

	time spent within a ± 15 cm strip centered on path #3
with non-linear control law (29)	16 %
with adaptive control law (35) and MRAC scheme	59 %
with adaptive control law (35) and IMC scheme	70 %

It can be observed on Table 4 that adaptive control law (35) relying on IMC scheme leads to a more accurate path #3 following than when it relies on MRAC scheme (70 % vs. 59 %). The difference in the performances of these two guidance laws is even more significant when considering Figure 29(a): when adaptive guidance law (35) relies on MRAC scheme, the farm tractor presents larger oscillations than when it relies on IMC scheme. These larger oscillations originate from the delay in accounting properly for sliding effects, that it is slightly larger with MRAC scheme than with IMC scheme: in MRAC scheme, the adaptive corrective term y_c is obtained from a simulation application. Changes in sliding parameters \dot{Y}_P and $\dot{\Theta}_P$ require then some delay prior to be reflected in y_c value. In contrast, in IMC scheme, the adaptive corrective term y_c is derived from asymptotic relation (34). Therefore, even if this y_c value has to be filtered, changes in sliding parameters \dot{Y}_P and $\dot{\Theta}_P$ can be reflected within a shorter time. When the vehicles are moving on a sloping field, sliding conditions change in a faster way than when they are describing curves on a level ground. Therefore, differences between IMC and MRAC schemes, that were not obvious in the latter situation, appear more clearly in the former one. The small delay introduced by MRAC scheme when accounting for sliding, is compensated via higher steering angle values, as it can be observed on Figure 29(c). Higher steering angle values lead necessarily to higher angular deviations, see Figure 29(b). Therefore, the vehicle trajectory presents more oscillations when MRAC scheme is used, rather than when adaptive control law (35) relies on IMC scheme, as it can be observed on Figure 29(a).

6 Conclusion

The aim of this work was to provide agricultural vehicles with automatic guidance capabilities, relying on an RTK GPS as the single vehicle sensing device. More precisely, accurate curved path following on agricultural fields where sliding is likely to occur, was addressed.

Since sliding effects have to be taken into account, a natural approach would have been to design guidance laws from a vehicle dynamic model. However, in as harsh conditions as are agricultural ones, these very large models, enclosing numerous badly known and

even varying parameters, do not appear very tractable. It has been shown here that, as an alternative, sliding effects on vehicle motion can be satisfactorily accounted by an extended kinematic model, derived by introducing an additive structured perturbation into a vehicle kinematic model designed under pure rolling and non-sliding conditions at wheels-ground contact points.

Capability of the single RTK GPS sensor to provide online the state and perturbation vectors of that extended kinematic model has then been discussed. State vector, i.e. vehicle relative location and relative heading with respect to the reference path, can clearly be inferred from the position measurements supplied by this sensor, but heading information have nevertheless to be proceeded through a Kalman state reconstructor in order to improve its accuracy and then enable its use inside guidance laws. Perturbation vector can also be satisfactorily estimated, by comparing the actual vehicle position supplied by the RTK GPS sensor, with its expected position when sliding does not occur, obtained from online simulation.

Vehicle guidance laws design, relying on that extended kinematic model, has then been carried out according to three steps. First, it has been assumed that the vehicles do not slide. In that case, their kinematic model can be converted into a so-called chained-form, from which very attractive non-linear control laws can be designed: high accuracy curved path following can then be achieved, since both vehicle model non-linearities and path curvature can be explicitly taken into account. In addition, although these guidance laws are non-linear ones, performances tuning can still be achieved as intuitively as in the linear systems case. Moreover, these performances can be set independently from the vehicle velocity, which is a very interesting feature from a practical point of view.

Next, since in vehicle extended kinematic model, sliding effects are described as a perturbation term, it has been possible to account for them via adaptive control techniques. More precisely, relying on internal model approach, an adaptive corrective term has been introduced into previous non-linear control laws: guidance accuracy can then be ensured despite sliding occurrence, at least when sliding effects are slowly varying, while all the attractive features of non-linear guidance laws are still preserved.

Finally, in order to ensure guidance accuracy even when sliding effects present large variations (e.g. at the beginning/end of a curve), some anticipation has to be provided to the control laws, in order to counterbalance for the delays enclosed in the guidance feedback loop, mostly due to the actuator device. Future values of the reference path curvature are obvious data on which anticipation can efficiently rely. Model predictive control techniques have been shown to be a relevant approach to incorporate such an anticipation into the above designed guidance laws, and therefore to preserve their accuracy even at curvature path discontinuities.

Capabilities of the proposed guidance laws have been extensively investigated via numerous full-scale experiments. The first ones have been carried out on an asphalted ground. The aim was to achieve path following in a very favorable situation where the farm tractor does not undergo sliding, so that all the attractive features of the non-linear control laws can easily be highlighted. Then, experiments on agricultural fields have been performed, and

much more unfavorable situations, where the farm tractor undergoes severe sliding, have been considered: namely, sharp curve following on a level slippery ground and straight line following on a sloping field. These experiments have demonstrated the capabilities of the adaptive control scheme to preserve guidance accuracy despite sliding occurrence, and abilities of predictive control scheme to avoid transient guidance error at sliding discontinuities.

Current continuation of this research work aims at introducing some additional improvements, on one hand by addressing modeling refinements, and on the other hand by extending at minimum vehicle sensing device.

Modeling refinements are first investigated in order to provide with more accurate values for the vehicle heading. For the present moment, both raw vehicle heading measurements and Kalman state reconstructor equations rely on pure rolling and non-sliding conditions at wheels-ground contact points, which is obviously not completely satisfactory. In some unfavorable situations, such as straight line following on a sloping field, the accuracy of vehicle heading values is even significantly damaged, since the vehicle is continuously moving crabwise, as it has been observed on the experimental reports. Another concern when measuring vehicle heading are tractor cabin oscillations: tractor roll and pitch are not accounted for the present moment. However, they slightly damage position measurements, and by propagation, damage more seriously vehicle heading values, especially when the vehicles are moving on irregular ground. Therefore, more comprehensive models, accounting for these effects, are currently considered in order to support vehicle heading evaluation, that would be derived from these models according to observers (such as Luenberger).

Modeling refinements are also addressed with the aim to obtain more representative values for sliding variables. For the present moment, they are derived from the comparison between the vehicle actual position, provided by the RTK GPS sensor, and the vehicle expected position if it had not undergone sliding, supplied from online simulation. Such an estimation is however not always totally relevant, since any perturbation on vehicle position measurement (and firstly when the tractor undergoes roll and/or pitch) is directly propagated to sliding variables values: for instance, when a vehicle crosses a hole on the ground, the tractor cabin is shaken, the vehicle actual and expected positions do not fit, and therefore sliding is detected when it has not to be. Other dynamic phenomena, such as delays originating from the vehicle large inertia, can also generate inconsistencies between the vehicle actual and expected positions, and then lead to misinterpreted sliding effects. Therefore, more comprehensive models which could provide with more representative values for sliding variables, are also currently investigated.

Finally, modeling refinements are also developed in order to improve the efficiency of prediction algorithms. At the present moment, only the steering actuator model is explicitly used when deriving the anticipation to be introduced in guidance laws, with respect to the future values of the reference path curvature. However, some other dynamic phenomena also generate delays in guidance feedback loop, and firstly those originating from the large vehicle inertia. In the experiments reported above, they are implicitly accounted since the prediction horizon has been empirically extended. Nevertheless, a more efficient an-

ticipation could obviously be provided if more comprehensive models, incorporating these dynamic features, were used explicitly in prediction algorithms.

All the above mentioned modeling refinements are devoted to estimation and prediction purposes: they aim at accounting explicitly for dynamic features in order to either improve the accuracy of some variables describing the vehicle configuration, or to improve the models used in prediction algorithms. Vehicles dynamic models are however not expected to be used for control design purposes: the extended kinematic model presented here appears actually very tractable, since it allows to benefit from all the attractive features of guidance laws designed when it is assumed that the vehicles do no slide, while nevertheless accounting very efficiently for sliding effects.

In order to extract reliable information from these partial vehicle dynamic models, some additional measurements have clearly to be introduced: it does not appear possible to reconstruct with a satisfactory accuracy a larger vehicle attitude solely from the 3D position measurements supplied by a single RTK GPS. A minimum additional sensing equipment, which would enable to design efficient observers from partial dynamic models, is currently investigated. Theoretical developments (such as evaluation of observability rank conditions) and experimental characterization of the performances of some sensors in agricultural conditions, are being carried out.

References

- [1] T. Bell, M. O'Connor, V.K. Jones, A. Rekow, G. Elkaim, and B. Parkinson. Realistic autofarming closed-loop tractor control over irregular paths using kinematic GPS. In *Proc. of the European Conference on Precision Agriculture (ECPA)*, 1997.
- [2] P. Borne, G. Dauphin-Tanguy, F. Rotella, and I. Zambettakis. *Commande et optimisation de processus*. Series: Méthodes et pratiques de l'ingénieur. TECHNIP Editions, Paris, 1990.
- [3] C. Debain, T. Chateau, M. Berducat, P. Martinet, and P. Bonton. An help guidance system for agricultural vehicles. *Computers and Electronics in Agriculture*, **25**(1-2):29–51, 2000.
- [4] E. Dormegnie, G. Fandard, G. Mahajoub, and F. Zarka. *Dynamique du véhicule*. Lectures at French Institute for Advanced Mechanics (IFMA), Clermont-Ferrand, France, 2002.
- [5] M. Ellouze and B. d'Andréa Novel. Control of unicycle-type robots in the presence of sliding effects with only absolute longitudinal and yaw velocities measurement. *European Journal of Control*, **6**:567–584, 2000.
- [6] A. Gelb. *Applied optimal estimation*. MIT Press, Cambridge, MA, 1974.
- [7] T. Holzhüter and R. Schultze. Operating experience with a high precision track controller for commercial ships. *Control Engineering Practice*, **4**(3):343–350, 1996.

-
- [8] R. Lenain, B. Thuilot, C. Cariou and P. Martinet. Adaptive control for car-like vehicles guidance relying on RTK-GPS: rejection of sliding effects in agricultural applications. In *Proc. Intern. Conf. on Robotics and Automation (ICRA)*, pages 115–120, Taipei, 2003.
- [9] R. Lenain, B. Thuilot, C. Cariou and P. Martinet. Rejection of sliding effects in car-like robot control. Application to farm vehicle guidance using a single RTK GPS sensor. In *Proc. Intern. Conf. on Intelligent Robots (IROS)*, pages 3811–3816, Las Vegas, 2003.
- [10] H. Loeb. *Engin nautique de surface robotisé : synthèse de lois de commande et GPS différentiel*. PhD thesis, University of Bordeaux I, France, 1996.
- [11] R. Lozano and D. Taoutaou. *Identification et commande adaptative*. Hermes, Paris, 2001.
- [12] Y. Nagasaka, R. Otani, K. Shigeta, and K. Taniwaki. Automated operation in paddy fields with a fiber optic gyro sensor and GPS. In *Proc. International Workshop on Robotics and Automated Machinery for Bio-Production (Bio-Robotics)*, pages 21–26, Valencia (Spain), 1997.
- [13] M. O’Connor, G. Elkaim, T. Bell, and B. Parkinson. Automatic steering of a farm vehicle using GPS. In *Proc. International Conference on precision agriculture*, pages 767–777, Mineapolis (USA), 1996.
- [14] J. Richalet. Industrial applications of model based predictive control. *Automatica*, **29**:1251–1274, 1993.
- [15] J. Richalet. *Pratique de la commande prédictive*. Traité des nouvelles technologies série automatique. Hermes, Paris, 1993.
- [16] J. Ried and D. Niebuhr. Driverless tractors. *Ressource*, **8**(9):7–8, 2001.
- [17] C. Samson. Control of chained systems. Application to path following and time-varying point stabilization of mobile robots. *IEEE Transactions on Automatic Control*, **40**(1):64–77, 1995.
- [18] H. Sussmann, E. Sontag, and Y. Yang. A general result on the stabilization of linear systems using bounded controls. *IEEE Transactions on Automatic Control*, **39**(12):2411–2425, 1994.
- [19] B. Thuilot. *Contribution à la modélisation et à la commande de robots mobiles à roues*. PhD thesis, Ecole des Mines de Paris, France, 1995.
- [20] O. Yukumoto, Y. Matsuo, and N. Noguchi. Robotization of agricultural vehicles. *Japan Agricultural Research Quaterly (JARQ)*, **34**(2), 2000.
- [21] The Zodiac. *Theory of robot control*. C. Canudas de Wit, B. Siciliano, G. Bastin editors, Springer-Verlag, Berlin, 1996.